Diabatic Forcing and Initialization with Assimilation of Cloud and Rain Water in a Forecast Model: Methodology

By

William H. Raymond*, William S. Olson* and Geary Callan+

*Cooperative Institute for Meteorological Satellite Studies
1225 West Dayton Street
University of Wisconsin
Madison, Wisconsin 53706

+ National Environmental Satellite Data and Information Service (NOAA)
Madison, Wisconsin 53706

Submitted to *Mon. Wea. Rev.*

Abstract

In this study diabatic initialization and assimilation techniques are tested in a semi-implicit hydrostatic forecast model containing explicit representations of cloud and rain water. Diabatic vertical mode initialization and a diabatic forcing process are combined to strengthen the diabatic signal and to help the forecast keep the modification. In some experiments explicit cloud and rain water fields are retained through the analysis/initialization phase of the forecast cycle, i.e., from the end of one forecast to the beginning of the next sequential forecast, to help reduce the spin-up time of major precipitating events. This is only possible when these variables are explicitly computed and retained for use in prognostic cloud and rain water calculations. Deficiencies in the forecast model's production of precipitation can be reduced provided liquid cloud and rain water data are available.

Numerical experiments for a wide range of grid scale sizes, varying from 150 to 40 km, illustrate the adaptability of the diabatic initialization, diabatic forcing and liquid water assimilation procedures in combination with explicit cloud and rain water calculations. Particulars include information about the simple explicit cloud scheme and the diabatic initialization and diabatic forcing procedure. Presented also are comparisons between forecasts computed with the diabatic initialization, diabatic forcing and retained cloud and rain water fields and those obtained by the traditional adiabatic approach.

1. Introduction

In this investigation the primary goal is to identify one or more general procedures that will help reduce the time taken by numerical weather prediction models containing explicit cloud and rain water formulations to initiate or spin-up precipitation processes. These precipitation intensifying procedures also assist in enhancing the storm intensity. If the conventional data base could explain the atmospheric mesoscale flow in detail, then much of our problem would be eliminated. But the data base is primarily synoptic scale, requiring that a solution must be sought either in nonconventional data, in methods to initialize mesoscale circulations or by procedures that retain the model generated mesoscale dynamics and precipitation fields between the end of a forecast and the beginning of the next sequential forecast. All three methods are investigated in this study. These methods would allow the existing nonconventional data base, including satellite estimates of precipitation rate, to become more valuable for fine tuning and correcting model inaccuracies and conventional data shortcomings.

In this study we examine in a mesoscale regional model the initialization and assimilation of explicit cloud and rain water quantities. Parameterizations of the physical processes of condensation, evaporation, autoconversion, accretion and the removal of rain water by fallout are all included as source and sink terms in the liquid water conservation equations. The question of how to initialize the explicit liquid water calculations in numerical models and how to retain information about precipitation processes during the 4-D assimilation cycle are important issues that will be addressed. The explicit cloud model has purposely been kept simple so that different initialization techniques can be easily and economically tested.

With increasing computer speed there has been a slow but steady enhancement in model horizontal grid resolution. Current global numerical weather prediction models are approaching the spatial resolution where time-dependent cloud variables are physically relevant. The time to study the feasibility of initializing and assimilating cloud and rain water using explicit cloud conservation equations within a regional mesoscale model is now. The knowledge of explicitly

calculated cloud and rain water fields as a function of time and space provides information, such as model heating rates and vertical distributions, that are more difficult to obtain from conventional cloud parameterization approaches where cloud properties are not retained or used in a prognostic manner.

Cloud and rain water are the cumulative products of the transport of atmospheric moisture, both vapor and liquid, plus the physical processes included in cloud development and decay. By their very nature cumulative processes are difficult to initiate in numerical models, and it is common for precipitation to be absent during the first few hours of a numerical forecast. One reason for this deficiency is the resolution of the data. Conventional surface and upper air reports are frequently unable to capture the essence of mesoscale circulations with their enhanced convergence which supports the mesoscale precipitation process. The analysis of the irrotational wind component in the tropics is especially poor (Mizzi and Kasahara 1989). In mid-latitudes the large scale part of the irrotational wind can be estimated fairly accurately (Kasahara et al. 1992) but the mesoscale component depends a great deal upon the diabatic term (Tarbell et al 1981). The missing mesoscale circulations also influence the moisture and thermal fields (e.g., Krishnamurti et al 1984; Turpeinen 1990). Consequently, in order to initiate precipitation and assimilate cloud parameters it is necessary to know additional information beyond the conventional synoptic data base. This might include accurate estimates of the vertical heating rates and the low level convergence and/or the high level divergence that produces the cloud-sustaining vertical motion field. These also include the supporting mesoscale circulations that help produce long-lived disturbances. The incorporation of this data into model simulations is further complicated by inaccuracies or shortcomings in the forecast, e.g., phase errors.

When the heating rates are known or can be approximated, then either diabatic (Errico and Rasch 1988) or cumulus initialization (Donner 1988) is possible. These initialization procedures help establish circulation patterns consistent with latent heating processes that are otherwise not resolved in synoptic scale data. For a review of some studies using diabatic initialization schemes, see Table 1 in Turpeinen et al. (1990) and the introduction of Mathur et al (1992). Without the

heating rate information each forecast must go through a short time period where the mesoscale circulations that support precipitation processes must 'spin-up' before rainfall can be produced. In regional mesoscale models this spin-up usually occurs during the first 2 to 6 hours. Diabatic initialization should reduce the degree and duration of the spin-up, but this procedure is not always completely successful (Errico and Rasch 1988; Kasahara et al. 1992). In contrast, normal mode or dynamic initialization procedures, designed to help with the removal of gravity waves during initialization, only provide slight or no assistance in speeding up precipitation processes (Lejenas 1980).

Cloud and rain water data are generally not available. Rain gauge reports imply information about the total amount of liquid water reaching the surface, but no knowledge about the instantaneous vertical distribution is recoverable. Most microwave satellite measurements of instantaneous cloud quantities only resolve the vertically integrated cloud and/or integrated rain water. Thus it is necessary to make some assumption about the vertical distribution of the heating rate. New retrieval methods that combine observed microwave satellite radiances with cloud models should provide some insight into the vertical partitioning of the liquid water. These techniques are just beginning to be examined (Olson 1993).

The use of diabatic initialization requires an answer to the question of how the latent heating is going to be distributed in the vertical. Some studies have used representative profiles (Fiorino and Warner 1981; Puri and Miller 1990) others assume a general parabolic profile (Tarbell et al 1981; Salmon and Warner 1986, etc.) while some have tried to use the forecast model itself in some fashion with observations (Wergen 1988; Danard 1985; Turpeinen et al. 1990; Donner and Rasch 1989; Puri and Miller 1990; Heckley 1990). Donner (1988) used a variational formulation to optimize the vertical distribution with respect to the methodology of the Kuo cumulus parameterization. In all but the Donner study, it has been customary to use either the diabatic omega equation or a diabatic form of the normal mode initialization scheme. In contrast, Donner used a variational optimization.

Early pioneering work by Krishnamurti et al. (1984) suggested that in addition to the diabatic heating a re-analysis of the moisture and wind field is needed. Even earlier studies by Perkey (1976) and Wolcott and Warner (1981) enhanced the moisture field in cloudy regions. To produce the observed rainfall, Donner (1988) made slight modifications in the temperature field and relatively large changes to the humidity field. Donner and Rasch (1989) found that the divergence, temperature and moisture must all be adjusted to produce the proper precipitation. The necessity of moisture initialization to reduce the spin-up problem has also been noted in Turpeinen (1990) and Puri and Miller (1990).

The cumulus initialization used by Donner (1988) is effective in dealing with cumulus convective situations. However, improvements are still needed in the initialization of grid scale precipitation processes. In this study we use diabatic initialization, diabatic forcing, allow for moisture modification and in some experiments assimilate cloud water and rain water predicted by a forecast beginning 12 hours earlier. For the latter cases, non-zero cloud and rain water are carried through the 4-D data assimilation process from the end of one forecast to the beginning of the next forecast. The diabatic initialization is installed to work with the vertical mode initialization scheme of Bourke and McGregor (1983). Diabatic forcing is formulated in a new design to represent a natural continuation of the diabatic initialization. Together, diabatic initialization and diabatic forcing form a powerful system to reduce the time needed to spin-up precipitation processes and enhance storm development.

Theoretically, if precipitation data were always available then cloud and rain water could be treated much like other meteorological variables, i.e., updated and modified during the 4D assimilation process. However, caution is required when making large changes to existing model cloud fields, or to the dynamics that support the precipitation process. Testing and experience with explicit cloud initialization will dictate what the correct procedure should be. The problem goes far beyond any single study, and must be addressed in an operational setting where a large number of cases and situations can be examined over a long time period. Because of resource limitation

this study tests specific parts of the proposed initialization procedures separately, and then only on a few cases. The sensitivity of the initialization to the vertical distribution of the diabatic heating is appraised. Emphasized are procedures that have the potential to reduce the spin-up time and assist with enhancing storm development.

2. Modeling Considerations

A modified version of the Bureau of Meteorology Research Centre (BMRC) operational incremental O/I analysis (Mills and Seaman 1990), vertical mode initialization (Bourke and McGregor 1983), and semi-implicit forecast model (Leslie, et al. 1985) are used in this investigation. The incremental analysis is set to preserve the irrotational wind field while the rotational component of the differences between data and model guess wind and other fields are evaluated by the O/I. In this study the horizontal grid configuration varies from 40 to 150 km, while the vertical sigma coordinate is subdivided into 15 levels. The horizontal wind components, temperature and mixing ratio fields are smoothed with the 6th order implicit low-pass tangential filter (Raymond 1988), with a filter parameter setting sufficiently large enough to provide some horizontal mixing. Cloud and rain water quantities are not filtered, nor is horizontal diffusion applied to these fields.

Explicit conservation equations for cloud water and rain water are inserted in the model. The explicit cloud physics contain processes modeled using a modified Kessler type scheme (Kessler 1974), while the condensation and fall velocity calculations are similar to those described in Anthes, et al. (1987) and Liu and Orville (1969). The 'fallout' term is calculated by a semi-Lagrangian method to allow for the larger time steps used in the semi-implicit model calculations. Ice phase cloud physics have not yet been explicitly included in the model, but modifications are incorporated to increase the life time of high clouds and and to enhance anvil structures.

In sigma coordinates the frictionless explicit conservation equations for water vapor, cloud and rain water satisfy

(1a)

$$\partial(p^* q_v)/\partial t + \partial(up^* q_v)/\partial x + \partial(vp^* q_v)/\partial y + \partial(\dot{\sigma} p^* q_v)/\partial \sigma = p^*(P_{EVAP} - P_{CON}) + F_z ,$$

(1b)

$$\partial(p^* q_c)/\partial t + \partial(up^* q_c)/\partial x + \partial(vp^* q_c)/\partial y + \partial(\dot{\sigma} p^* q_c)/\partial \sigma = - p^*(P_{ACC} + P_{AUTO} - P_{CON}) + F_z ,$$

(1c)

$$\partial(p^* q_r)/\partial t + \partial(up^* q_r)/\partial x + \partial(vp^* q_r)/\partial y + \partial(\dot{\sigma} p^* q_r)/\partial \sigma = p^*(P_{ACC} + P_{AUTO} - P_{CON}) - g\partial(\rho q_r v_t)/\partial \sigma + F_z .$$

Here q_v, q_c and q_r are the water vapor, cloud water and rain water mixing ratios. P_{EVAP} is the evaporation of raindrops, P_{CON} is the condensation of water vapor (Asai 1965) or evaporation of cloud droplets, P_{ACC} is the accretion of cloud droplets by raindrops and P_{AUTO} represents the autoconversion of cloud droplets into raindrops. The acceleration of gravity is g, p^* is the surface pressure, ρ is the density of dry air and v_t is the mean terminal velocity of the raindrops. The independent variables t, x, y, and σ have their standard definitions. F_z represents the vertical diffusion. The map factor is omitted in the above equations.

Because of horizontal scale considerations, our explicit cloud calculations do not model individual clouds but yield approximate average values for a system or complex of clouds. This was the motivation behind the modifications made to the cloud physics formulation. It is known that the lifetime of individual convective clouds is less than one hour while a cloud complex exists for many hours with remnants lasting for days. Thus Kessler's (1974) accretion (collection) process was modified to slow the conversion from cloud to rain water when the cloud water q_c is below a preset critical value $q_c = C_{crit}$. Also incorporated into the accretion process is a vertical dependence on temperature that follows the scheme suggested by Schlesinger (1990). These changes help retain and enhance anvil or cloud top features. In addition to explicitly modeling

cloud complexes, the consequences of convection are parameterized by a modified Kuo-type cumulus parameterization scheme (Sundqvist et al 1989). However, in some cases the cumulus parameterization scheme is intentionally turned off to assist in the study of the spin-up of grid scale precipitation.

In mixing ratio units (gg^{-1}), the formula for the rate of change from accretion is

$$P_{ACC}=0.88C_1C_2\, q_c\, q_r^{0.875} \ , \tag{2}$$

where

$$C_1=\min[1.0,\ 1.0-(C_{crit}-q_c)/C_{crit}]$$

$$C_2=\max[0.0,\ \min(1.0,\ (T-233)/40)] \ .$$

Here T is the temperature in degrees Kelvin, and $C_{crit}=1\ gkg^{-1}$. Comparisons between model cloud water fields and infrared VISSR Atmospheric Sounder (VAS) images of cloud patterns and categories of low or high clouds, and SSM/I retrieved precipitation rates indicate acceptable ranges of cloud and rain water predicted by the explicit formulation. This will be shown later.

The autoconversion process is described by

$$P_{AUTO}=k_1(q_c-q_{co}) \ , \quad q_c \geq q_{co} \ ,$$

$$P_{AUTO}=0 \ , \quad q_c < q_{co} \ . \tag{3}$$

The parameters $k_1=10^{-3}\ s^{-1}$ and the onset of autoconversion depends on the critical value q_{co} which has the value of $0.2\ g\ kg^{-1}$.

To facilitate the large time step used in the semi-implicit forecast model the fallout term in (1c) is rewritten as two terms, one of which represents vertical advection, i. e.,

$$g\partial(\rho v_t\, q_r)/\partial\sigma \equiv A\partial(p^* q_r)/\partial\sigma + (p^* q_r g/p^*)\partial(\rho v_t)/\partial\sigma\,. \qquad (4)$$

Here A (s^{-1}) is equivalent to a velocity in the vertical σ coordinate system, that is

$$A = g\rho v_t/p^*\,. \qquad (5)$$

Thus, the time tendency for $p^* q_r$ in (1c) is found by semi-Lagrangian procedures using (4) and (5).

3. The Diabatic Initialization and Diabatic Forcing Formulation

The diabatic initialization is installed into the forecast model to take full advantage of the semi-implicit method. This is accomplished by modifying the semi-implicit representation of the average temperature $T^{2\tau}$, computed from the thermodynamic equation (McGregor et al 1978; Leslie et al 1985), by adding the temperature contribution T_{EX} from a measured or approximated diabatic heat source. This redefines the average temperature at the appropriate grid points using

$$T^{2\tau} \equiv T^{2\tau} + T_{EX}\,. \qquad (6)$$

(This is approximately equivalent to adding to the thermodynamic equation a forcing term $T_{EX}/\Delta t$, and including it in the semi-implicit formulation.) This modified temperature is then used in the semi-implicit calculations of the finite difference averaged horizontal wind components and surface pressure. To avoid excessive evaporation, some upward adjustment of the relative humidity may be required during this process . The amount of moisture needed to satisfy the expected condensation requirements is $c_p T_{EX}/L$, where c_p is the specific heat for constant pressure and L is

the latent heat of condensation. When cloud and rain water are assimilated it is especially important to retain saturation at the appropriate levels. During the vertical mode initialization procedure (Bourke and McGregor 1983), T_{EX} is held constant at the selected grid points. Recall, that the averaging in (6) for the semi-implicit method, with any variable χ, is defined by

$$\chi^{2\tau} = [\chi^{\tau+1} + \chi^{\tau-1}]/2 \ . \tag{7}$$

Following the initialization, the immediate application of an external diabatic forcing represents a natural extension of the diabatic initialization. Wang and Warner (1988) showed that this was useful. To keep the forcing from becoming excessive, the grid point average temperature is modified by the difference between the external contribution T_{EX} and the model produced or internal diabatic temperature change $T_{IN}=\Delta t L Q/c_p$, yielding

$$T^{2\tau} \equiv T^{2\tau} + (T_{EX} - T_{IN}) . \tag{8}$$

Here Q is the model produced condensed rate and Δt the time step. In our study the quantity in parenthesis in (8) is taken to be non-negative. If T_{IN} exceeds T_{EX} at a given grid location and timestep, then the forcing is reduced to zero. At some time in the forecast this would be the desired result but, it is not explicitly required before the termination of the forcing at a preselected forecast time. Too much forcing can over-develop the updraft and the liquid water content and/or create excessive gravity waves. The inclusion of the internally generated latent heating in (8) helps reduce over-development.

Note that (6) and (8) are similar, except that in (8) model produced condensation reduces the external forcing. This diabatic forcing is a natural continuation of the diabatic contributions used in the initialization. Thus, it is applied starting with the first time step after the vertical mode initialization and continued until the model produces an equivalent temperature change or until the

termination time is exceeded. This procedure is illustrated in Fig 1a.

To simulate the movement associated with a disturbance, T_{EX} is advected by the model horizontal winds according to

$$\partial(T_{EX})/\partial t + u\partial(T_{EX})/\partial x + v\partial(T_{EX})/\partial y = 0. \quad (9)$$

In regions with strong vertical shear it may be advantageous to advect T_{EX} using a vertically averaged horizontal wind. The advection process will ultimately smooth and diffuse the heating if (9) is used over a sufficiently large time period. Normally, the diabatic forcing is not applied long enough for this to become a problem. Albeit, to avoid noise some tapering is required to terminate the diabatic forcing, provided (8) is not reduced to zero by model generated condensation processes. Remotely sensed time variations in T_{EX} could also be specified if these were known. In their absence, the advection of T_{EX} is necessary to approximately locate the condensation. In our calculations T_{EX} remains unchanged except for horizontal advection. Thus, in this study the application of the external forcing is somewhat different from the procedure used in Newtonian nudging (Hoke and Anthes 1976).

An alternative approach, examined in this study, is to apply the external diabatic forcing at the satellite observation time without reinitializing the model, i.e., with no diabatic initialization. Then, during the forecast, a gradual transition into and exit from the external forcing greatly avoids the production of noise and gravity waves. This is shown graphically in Fig 1b to contrast how this procedure differs from diabatic initialization. The time span needed to produce gradual changes depends upon the magnitude of the external forcing. The length of the time period used in the forcing can be varied to achieve the desired result. Excessively long periods of forcing should be avoided since they can can lead to some negative consequences. For example, overproduction of precipitating liquid in the atmospheric column leads to down bursts accompanied by low-level divergence, ultimately choking off the moisture source.

In any event, the horizontal distribution of the forcing is determined using the grid

configuration and knowledge of the location of the storm or liquid precipitating water. In the absence of measurements, the best vertical placement of the forcing remains unknown and is a function of several factors, including the nature of the disturbance. For example, hurricanes are known to be warm core; warming extends to surface, while most middle-latitude disturbances have upper level lows with warming that does not extend to the surface (Wallace and Hobbs 1977).

Raymond (1993) has identified diabatic wind modifications that induce secondary vertical circulations that contribute to the convergence, helping to create or support long-lived mesoscale flows. An approximate representation for the secondary flow within the diabatically active part of the disturbance, based on near conservation of the large scale kinematic moisture flux, requires that the x and y coordinate horizontal wind components u and v be modified by the addition of a perturbation term of the form

$$u_{pert} = R_1 v_g - R_1^2 u_g + \cdots \quad , \tag{10}$$

$$v_{pert} = -R_1 u_g - R_1^2 v_g + \cdots \quad . \tag{11}$$

Here $R_1 = -|Q/(fq)|$, Q is the condensation rate, f is the Coriolis parameter, q the mixing ratio and u_g and v_g are the geostrophic wind components for u and v respectively. Generally R_1 is small, say, $0 < R_1 < -0.50$. Because (10) and (11) only describe the modifications within the updraft, they represent only part of an unbalanced ageostrophic approximation of the mesoscale circulation. Theoretically, a balanced and complete flow can be determined, but this requires additional computational resources to solve a vorticity equation. In our calculations, R_1 in (10) and (11) is used as an independent gauge to measure the production of latent heating, but the wind field is not modified.

4. Precipitation Events

Precipitation spin-up processes associated with three different weather phenomena are examined. The first situation includes a tropical disturbance known as Emily. The initial conditions are taken from NMC's initialized global data set beginning at OOOO UTC 21 Sept. 1987. At that time Emily was a tropical storm located among the Windward Islands a little ways south of the Island of Martinique, just north of the Venezuelan coast in the Atlantic Ocean. The model calculations are performed on a 65 x 65 horizontal grid with 40 km grid spacing, having 15 vertical sigma levels. The time step size used in the semi-implicit model is 300 s.

The second major precipitation study examines rapid cyclonic development in the North Atlantic. Intensive observation period number five (IOP-5) is selected from the Experiment on Rapidly Intensifying Cyclones over the Atlantic (ERICA). It represents a case where a major cyclone over water experiences a rapid pressure deepening. Our examination extends from 0000 UTC 19 January 1989 through 0000 UTC on the 20th. For this part of the study the forecast model uses a horizontal grid resolution of 120 km. The initial meteorological fields for our ERICA IOP-5 case study are obtained from NMC's initialized global analyses. Conventional data are limited because the disturbance is located over water. However, observations during ERICA have documented the cyclone's path, pressure and provided an assortment of other atmospheric measurements using dropsondes and aircraft. Also, the microwave measurements of the precipitation rates retrieved from the Special Sensor Microwave/Imager (SSM/I) provide a product of major importance in verifying the precipitating liquid in the forecast.

The final precipitation event used to study model spin-up comes from a time period that includes frontal development associated with strong wind jets over the US. Specifically, 24h forecasts are made for the period beginning 1200 UTC 21 April 1988. This case over North America was selected because of its large conventional data bases including surface, upper air and aircraft winds. The horizontal grid scale used in this part of the modelling effort is 150 km on a 35 x 35 grid with 15 vertical sigma levels.

5. Discussion of Results

A. Tropical Storm Emily

Super-imposed over the validating GOES infrared (IR) image of tropical storm Emily in Figs 2 and 3 are the 700 mb geopotential height and divergence fields, respectively, from a fourteen hour forecast beginning at 1000 UTC 21 September 1987. The forecast uses an adiabatic initialization with four vertical modes and the initial meteorological fields come from a ten hour preforecast. Decreasing the number of modes by one or two makes no significant difference in the adiabatic initialization. Note in Figs 2 and 3 that the height and divergence fields show very little development whatsoever in the immediate vicinity of Emily. A small trough is located to the east of Emily in Fig 2, but no precipitation is produced over any water surface, although moderate amounts of precipitation fall in some elevated regions.

In the absence of the model's inability to produce any diabatic heating in the vicinity of Emily during a 10 h preforecast beginning 0000 UTC 21 Sept 1987, a proxy latent heating field is assigned based on the approximate position of Emily in the 1001 UTC satellite image. (In a separate study that will be presented elsewhere, data from SSM/I estimates of the precipitating liquid and ice at 1000 UTC 21 Sept 1987 are used in initialization experiments) In this study highly simplistic initial conditions are used to test our basic diabatic forcing procedure. Previous investigators have also used simplified approaches to describe the vertical distribution of the latent heating, including Tarbell et al (1981), Salmon and Warner (1986), Ninomiya and Kurihara (1987), and Wang and Warner (1988). Our proxy temperature distribution is described by the product of vertical and horizontal sine functions, viz.,

$$T_{EX}=K \sin(a\pi)\sin(b\pi)\sin(c\pi) \qquad (12)$$

where K is the maximum magnitude of T_{EX} and $a=(k-k_T)/(k_B-k_T)$, $b=(j-j_S)/(j_N-j_S)$ and $c=(i-i_E)/(i_W-j_E)$. The independent coordinates i, j, and k are associated with the x, y and σ variables, respectively. At 1001 UTC 21 September 1987, Emily was approximately centered

near grid point location (40.5,30.5) in our 65 x 65 horizontal grid. Assigning j_S=26, j_N=35, i_E=37, i_W=44 and setting K=0.5 gives the distribution shown at 500 mb in Fig 4, provided the sigma levels are between 0.25 and 0.80. This vertical distribution is compatible with pre-hurricane/tropical wave observations (Kuo and Raymond 1980; Shapiro and Stevens 1980). In general, the values for k_B and k_T are varied to test the impact of heating at different vertical heights.

Figures 5 through 7 contain fields from a fourteen hour forecast using the diabatic initialization and a two hour application of diabatic forcing as described in (6) through (12), and illustrated in Fig 1a. For convenience, diabatic initialization will be denoted by DI, while DF(K) will identify diabatic forcing with a maximum temperature perturbation of K degrees. The 700 mb height field from the fourteen hour forecast, Fig 5, contains closed contours of small magnitude over the southern extent of tropical storm Emily, indicating that the forecasted disturbance still has a cold core. The 700 mb vorticity, with maximum in excess of 2 x 10^{-4} s^{-1} is similarly located (Fig 6), while the 700 mb divergence (Fig 7) is positive directly behind the disturbance and negative (convergence) within the vicinity of the storm and to the southwest. The diabatic temperature perturbation used in these calculations has a maximum value of K=0.5 C per time step of 300 s. Six iterations (iter=6) are used in the vertical mode initialization (Bourke and McGregor 1983), each having a time step of 50s, requiring that K be modified appropriately in the initialization, i.e., K=0.5/iter. In (12), the parameters describing the vertical depth of the perturbation are assigned k_B=9 and k_T=3, i.e., the forcing occurs between sigma levels 0.25 and 0.80. Also, the diabatic forcing, which is applied over a time period of two hours, is ramped linearly to zero during the second hour.

Four vertical wave numbers are used in the initialization shown in Fig. 8. Included in this figure are curves describing the number of grid scale condensation points per time step for adiabatic, diabatic initialization (DI), and for two different time periods of diabatic forcing (DF). Note that, without the diabatic forcing, the diabatic initialization is unable to produce sustained condensation activity over the fourteen hour forecast. This is true for vertical modes 2 and 3 also.

Adding additional moisture during the initialization at all locations influenced by the diabatic heating does not enhance the long term development. However, strong diabatic activity occurs when the diabatic initialization is combined with diabatic forcing, where the forcing is applied for a duration of either two or three hours. In Fig 8 note that the longer the diabatic forcing is applied, the more intense is the storm development as gauged by the production of precipitation. Both the diabatic initialization and diabatic forcing are restricted to the immediate Emily region which is entirely over water, as illustrated in Fig 4. Thus, the difference between the adiabatic and other curves represent development in the Emily region. In fact, the development wants to become too extreme, partially because of the large availability of moist air in this tropical location, and partially because the natural tropical storm circulation, feedback and balancing processes, developed over several days, are difficult for the model to duplicate in a few hours. To keep the storm from over developing or developing too rapidly, the maximum amount condensed at any one time step at any grid location is restricted by requiring that $-0.5<R_1<0$. Conservation of moisture is retained since the excess is carried in the slightly super saturated mixing ratio. This is thought to be a better alternative than applying artificial diffusion which is non-conservative. It is also consistent with the fact that small sub-grid scale moist and dry downdrafts exist within the cloud environment, limiting to some extent the updraft while enhancing mixing, thereby reducing the condensation amount. Except for the K-theory vertical diffusion, these processes are not explicitly included in the conservation equations (1a,b,c) or in the condensation calculation, but should be parameterized in some way.

In our calculations the horizontal wind is required to spin-up through time since the disturbance is initially absent, and since no bogus tropical storm wind field is inserted during the initialization. At non-tropical latitudes it has been shown that a perturbation spiral feature associated with a mean converging flow has an e-folding times in excess of 22 hours (Raymond 1989) as a consequence of vortex stretching (mean divergence of 10^{-5} s). Still, in model simulations performed by Kurihara and Tuleya (1981), the development of a deep vortex

characteristic of a tropical storm from a shallow easterly wave required three to five days.

The mesoscale circulation pattern associated with the tropical storm also influences the diabatic activity. When the relative vorticity is of the same order as the planetary vorticity, then the surface pressure tendencies are influenced very little by diabatic heating (Delden 1989). But, the more intense the vortex, the greater the response to a given heat source (Schubert and Hack 1982; Delden 1989).

Figure 9 shows that when diabatic forcing is used, the number of vertical modes in the initialization has little influence on the grid scale condensation. But the magnitude of the forcing is shown to be influential, as illustrated by the difference between the DF(0.3) and DF(0.5) curves. Clearly, the greater the forcing the greater the response. Also in Fig 9 it is seen that when the forcing is closer to the surface, i.e., between sigma levels 0.4 and 0.95, the response is greater, presumedly because more moisture is transported vertically.

In Fig 10 a maximum of 14.26 cm of precipitation is recorded over fourteen hours when the forcing DF(0.5), centered between sigma levels 0.25 and 0.80, is applied for two hours. Approximately fifty percent more rainfall is recorded when the forcing is extended in duration from two to three hours. As expected, reducing the maximum magnitude of the forcing from K=0.5 C per 300 s time step to 0.3 C reduces the rainfall, yielding a maximum of 4.59 cm for DF(0.3). When the forcing is placed lower in the atmosphere, i.e., between sigma levels 0.4 and 0.95, then more moisture condenses and more total precipitation falls, but for this case the maximum rainfall is nevertheless reduced. Generally, Fig 10 shows that a high degree of correlation exists between the number of grid scale condensation points, shown in Figs 7 and 8, and the maximum rainfall. To help visualize the precipitation pattern the rainfall recorded on the surface, associated with a two hour application of DF(0.5), is shown in Fig 11. The convective rainfall resulting from the cumulus parameterization is small in this region (not shown), although the 40 km grid resolution is somewhat boarder line for the effective use of a Kuo-type cumulus parameterization scheme.

The diabatic forcing can also be used at any time during a forecast as shown graphically in

Fig 1b. For example, results from an application of diabatic forcing beginning ten hours into a twenty-four hour forecast, as the sole means to enhance the spin-up of tropical storm Emily, are illustrated in Figs 12 through 15. Beginning the application of diabatic forcing DF(0.25) in nearly the middle of a forecast at the satellite observation time, with the forcing centered between $0.25 < \sigma < 0.80$, requires a gradual approach into and decline out of the forcing regime to avoid introducing noise. A time period of one and one-half hours (time steps 120 to 138) is selected for linearly introducing the forcing, which remains constant for one and one quarter hours (time steps 138 to 153), while one hour (time steps 153 to 165) is used to turn off the diabatic forcing. The resulting geopotential heights contain closed contours (Fig 12), while significant vorticity ($>2.5 \times 10^{-4}$) and convergence are revealed in Figs 13 and 14 respectively. Convergence even exists in the region containing the spiral arm in the satellite image. The placement of these features is fairly good. A maximum rainfall of 94.5 mm is indicated in Fig 15. In the control, no rainfall is produced in the region containing Emily, but over 90 mm falls on the mountain slopes. Figure 15 also shows that doubling the forcing doubles the rainfall while low-level forcing gives a large maximum of 277.2 mm. The areal distribution of the precipitation produced by the twenty four hour forecast, using DF(0.25) (solid line), and the low level forcing (dashed line), is given in Fig 16 and are somewhat reduced in comparison with the precipitation from the fourteen hour forecast shown in Fig 11.

The number of grid scale condensation points as a function of time is shown in Fig 17 for the control (no forcing), and for three different vertical distributions and two different magnitudes of diabatic forcings. The grid scale condensation points occurring in the control case are associated with convection over elevated topography, none occurs in the vicinity of Emily. Differences then between the control and forced cases are associated with Emily. Figure 17 clearly shows that the magnitude of the forcing is important.

Presented in Fig. 18 is the integrated precipitating water, in kgm^{-2}, predicted by the fourteen hour forecast. It can be compared with the SSM/I retrieved estimates (Olson 1993) given in Fig 19. Note the latter is distributed over a much larger area and contains a comma shaped pattern,

while the forecasted amount has concentric contours much like the shape of the forcing. The maximum produced by the forecast is slightly too far south. Enlarging the initial areal size of the diabatic heating results in a proportional increase in the integrated rain water in the fourteen hour forecast. When the initial conditions are shifted to the north, then the development in the forecast responds in a corresponding manner (not shown).

B. ERICA IOP-5

This case differs from the Emily situation in that the 12 hour preforecast produces diabatic activity over the region of interest. However, diabatic heating fields from the last time step of the 12 hour preforecast are thought to be unrepresentative enough that they should not be used directly in the diabatic initialization and diabatic forcing formulation. Consequently, the T_{EX} fields, with a maximum of <1 C during a 600 s time step, are set proportional to the coverage and vertical distribution of the cloud water fields (not shown) predicted by the 12h preforecast. It is assumed that the distribution of cloud water is more representative of the distribution of heating than the larger size rain water particles which fall out as precipitation.

Figure 20 illustrates, for a grid resolution of 120 km at 0000 UTC 20 1988, that the diabatic initialization produces a doubling of the negative omega values (solid lines) found at 700 and 400 mb in the global analysis. This initialization did enhance slightly the storm development and rainfall distribution in the 12h forecast, but the predicted 988 mb low pressure is far from the observed 968 mb measured in this rapidly deepening storm (IOP-5), as indicated in the ERICA Field Phase Summary (Hartnett et al. 1989). Thus, given the model's 120 km horizontal resolution, additional measures are required to better forecast this intensely developing storm.

Results from a 24h forecast, ending at 1200 UTC 20 Jan 1988, are compared in Figs 21, 22 and 23 against a control twelve hour forecast and with two diabatically forced cases. The diabatic forcing is applied to the global initial conditions, and in all calculations the cumulus parameterization scheme has been turned off to isolate the spin-up process for the grid scale

calculations. In Fig 21 the wind speed at 500 mb is shown. Note that the jet develops a maximum speed of 40^+ ms^{-1} in all cases except the lower right figure, which is from a forecast using four hours of diabatic forcing. This forecast produces 50^+ ms^{-1} wind speeds in the dry slot just behind the upper part of the comma. Note that two hours of diabatic forcing did increase the area under the 40 ms^{-1} curve (lower left). The change in the wind field can be directly associated with the enhancement in the comma shape of the mixing ratio shown at the 700 mb level in Fig 22. Note also in the two and four hour diabatically forced forecasts, that the gradients of mixing ratio are largest to the rear of the storm.

Fig 23 shows the precipitation (mm) accumulated during a twelve hour period. The final twelve hours of the twenty four hour forecast produced a small region with a maximum in excess of 70 mm, while the diabatically forced forecasts show a slight reduction in the maximum precipitation from 30^+ mm (upper right) to 20^+ mm. This small and temporary reduction is thought to occur because the continual diabatic forcing builds a deeper system containing more precipitating liquid aloft. If, however, the forcing is too strong or applied too long, then the upward vertical motion becomes large, causing an excessive amount of water to be suspended in the atmospheric column. Then, the eventual fallout of this rain water can lead to negative consequences, and possibly the premature death of the storm.

The area averaged precipitation rate as a function of time is presented in Fig 24 for five forecasts and from satellite measurements. The latter is computed using a technique (Martin et al 1990) that estimates the hourly precipitation rate from satellite infrared image cloud-top temperatures by a regression power-law formula. The coefficients in the power-law formula are obtained using maximum-likelihood correlations of relationships between cloud-top temperatures and a large number of raingauge precipitation rate observations (B. Goodman, personal communication). The variations seen in Fig 24 for the observations are small, but the extra time needed to spin-up the precipitation in the model is clear. In the legend in Fig. 24 "large scale" refers to the traditional method of instantaneously removing from the atmosphere water vapor in

excess of saturation. Clearly, this procedure needs less time to produce precipitation than the grid scale explicit cloud category which requires time for the different cloud processes to react and for the rain water to reach the earth's surface. Retaining cloud and rain water unaltered through an assimilation cycle (heavy solid line) allows the precipitation to continue at the same rate as it had previously, denoted by "hot start" in the legend. Note that all methods come close to converging to the average precipitation rate seen in the satellite measurements. The forecast that uses diabatic forcing for four hours (not shown) produces just slightly less rainfall than the explicit category with no diabatic forcing (open circle).

Super-imposed over the GOES 7 IR image at 1201 UTC 20 Jan. 1989 in Fig. 25 is the surface pressure field. This field is from a 12 h forecast that uses diabatic initialization (DI), consequently it deepens to only 988 mb instead of the observed 968 mb. In contrast, using the diabatic initialization (DI) and diabatic forcing (DF) over a 4 hour period, where during the last two hours the forcing is linearly tapered to zero, produces a 968 mb contour as shown in Fig 26. However, some gravity wave noise is also produced as can be seen by the waviness of the contours near the US coast and elsewhere.

C. US Forecasts (1200 UTC 21-22 April 1988)

The final case involves a meteorological situation where surface and upper air reports are plentiful. This situation was chosen to test how conventional data effects the assimilation of cloud and rain water quantities. Rainfall and other meteorological information for this time period is available in the Daily Weather Maps[1]. Generally, a stationary front is located over Colorado, Wyoming, and Montana, with the center of the surface low over Kansas. Another stationary front lying directly east of the surface low. The heaviest concentration of clouds are found to the north of the front. Rainfall amounts are generally light to moderate, with less than one-half of an inch over the last twenty-four hours. Upper level moisture and a band of high clouds have moved

[1] Daily Weather Maps, Weekly Series April 18-24, 1988, National Oceanic and Atmospheric Administration, National Weather Service, National Meteorological Center Climate Analysis Center.

across Mexico and into the southern US. Only a small amount of precipitation is associated with this upper level system. The integrated cloud water (x 100 kg m^{-2}) from our 12 hour forecast is shown in Fig 27, valid for 1200 UTC 22 April 1988. The predicted cloud cover is surprising good for the region north of the front, given the 150 km horizontal resolution use in the forecast. Boundary conditions influence the cloud development along the eastern, western and southern boundaries. The high level clouds along the southern part of the US are not predicted, partially because the southern boundary condition in our regional model calculations did not supply enough moisture. Initial conditions for this forecast used surface and upper air observations, along with the traditional model produced guess fields plus cloud and rain water information supplied by the 12 hour preforecast. These liquid water quantities helped reduce the time needed for precipitation to develop, as illustrated below.

Figure 28 illustrates the sensitivity of the vertical mode initialization procedure. Note that for two vertical modes the number of condensation points, in the grid scale calculations for a one time step forecast, change little when the magnitude of the heating is increased by a factor of four. However, the number of condensation points increases dramatically as the number of modes in the vertical mode initialization is increased. This requires that care must be exercised in selecting the proper number of vertical modes. When diabatic forcing is combined with the diabatic initialization, the importance of selecting the proper vertical modes is less important, as has been illustrated earlier. In the above calculations the T_{EX} fields are generated using cloud water information from the 12 hour preforecast.

Changes in the grid averaged precipitation rate resulting from the inclusion of data inserted during the assimilation cycle are contrasted in Fig 29 with the contribution from the cumulus parameterization process. Here MG stands for the preforecast model generated 150 km resolution fields used in the initial conditions, and represents a forecast that does not use cumulus parameterization unless so stated. Note in Fig 29 that the largest difference in precipitation production between the MG simulation with cumulus (thin line) and without cumulus (circle) exists

early in the forecast. Also clear in Fig 29 is the fact that precipitation contributions added by the cumulus parameterization are larger than the precipitation changes induced by the addition of the surface, upper air and air craft data (thick line). To really understand the impact of data, i.e., temperatures, pressures, mixing ratios, and winds upon the assimilation of cloud and rain water will require an examination of a large number of cases. Such a study must be conducted within an operational environment.

The number of grid scale condensation points (Fig 30) and the grid averaged precipitation rate (Fig 31) indicate large differences which exist between the global no data + DI and the other MG categories. For this particular case, at the 150 km resolution, the inclusion of cloud, cloud and rain, or cloud and rain water plus diabatic initialization (DI) makes a difference during the first half of the 12 hour forecast. These differences are still much less than those found between the global and the higher resolution MG data sets. Nevertheless, even in this situation which contains weak to moderate precipitation events, there are some positive benefits, seen especially in Fig 31, from including the cloud water in the assimilation cycle. Their inclusion also temporarily increases the total moisture supply, until it all is rained out. Also, diabatic initialization is usually required in the assimilation of cloud and rain water to help sustain or add to the supporting mesoscale circulation.

The amount of mesoscale resolution in the initial model fields makes a difference 12 hours later in the vertical distribution of the area averaged cloud and rain water, as shown in Fig 32 and 33. Note that the MG higher resolution initial fields produce cloud water in the 12 hour forecast that has a larger percentage of its total contribution at elevated sigma levels (Fig 32). Similar comments apply to the rain water displayed in Fig 33. This would seem to be a natural consequence of having enhanced vertical motions and larger magnitudes of convergence. The differences illustrated in Fig 32 and 33 also imply that diabatic temperature initialization, used with the global data is not able to correct for missing diabatic mesoscale circulation deficiencies.

VI Summary

In this study several methods are shown to enhance the development and reduce the spin-up of precipitation when explicit cloud and rain water calculations are used. These include diabatic initialization, diabatic forcing and the assimilation of cloud and rain water fields from one forecast to the next sequential forecast. To statistically validate any of the precipitation enhancing procedures requires an operational setting where a large number of cases can be tested.

Diabatic initialization can be given an assist by a short period of diabatic forcing following the initialization. This is also beneficial for enhancing storm intensity. The forcing procedure can be constructed to be a natural continuation of the diabatic initialization, but can be applied at any time provided care is taken to avoid introducing noise. Advection of the external heating field helps with the proper horizontal placement of the forcing provided the forecast wind field is approximately correct. Extra moisture can also be added to help encourage diabatic development. When explicit cloud schemes are employed, the assimilation of cloud and rain water from one forecast to the next sequential forecast has the potential to be a useful method for encouraging the early development of precipitation, especially in major disturbances. Improved modeling techniques using diabatic forcing and cloud and rain water assimilation are thus able to help reduce the spin-up of grid-scale precipitation and enhance mesoscale circulations, which in turn provide the support necessary to sustain continued diabatic activity.

The vertical placement of the diabatic forcing remains a difficult problem. Using the vertical levels and proportions of the cloud development in the preforecast provides some vertical information, but difficulties remain in regions that lack cloud development. Most of the time the lack of cloud development can be traced to the lack of information in initial conditions. This study shows that data assimilation, diabatic initialization and diabatic forcing procedures can be used with explicit cloud and rain water formulations to encourage, enhance and modify the cloud and rain water fields, and to intensify the forecasted storm development. A major problem is the lack of data to initialize the cloud and rain water fields and an incomplete knowledge of the correct vertical

profile of latent heating. Promising satellite retrieval techniques, that combine standard remote sensing procedures with physical models to estimate the precipitating liquid water and ice distributions, may also be able to estimate the vertical placement of the latent heating fields. This holds great promise for providing data for the assimilation of the initial cloud and rain water fields, especially over water surfaces.

Acknowledgments. This work was supported by NASA Grant NAGW-1855. One author (WHR) was supported in part by National Science Foundation Grant ATM-8920508.

References

Anthes, R. A., E-Y Hsie and Y-H Kuo, 1987: Description of the Penn State/NCAR mesoscale model version 4 (MM4). NCAR Technical Note NCAR/TN-282+STR. National Center for Atmospheric Research, Boulder, Colorado, 66pp.

Asai, T., 1965: A numerical study of the air-mass transformation over the Japan Sea in winter. *J. Meteor. Soc. Japan*, **43**, 1-15.

Bourke, W. and J. L. McGregor, 1983: A nonlinear vertical mode initialization scheme for a limited area prediction model. *Mon. Wea. Rev.*, **111**, 2285-2297.

Danard, M., 1985: On the use of satellite estimates of precipitation in initial analyses for numerical weather prediction. *Atmosphere-Ocean*, **23**, 23-42.

Delden, A. van., 1989: On the deepening and filling of balanced cyclones by diabatic heating. *Meteorol. Atmos. Phys.*, **41**, 127-145.

Donner, L. J., 1988: An initialization for cumulus convection in numerical weather prediction models. *Mon. Wea. Rev.*, **116**, 377-385.

_____, and P. J. Rasch, 1989: Cumulus initialization in a global model for numerical weather prediction. *Mon. Wea. Rev.*, **117**, 2654-2671.

Errico, R. and P. J. Rasch, 1988: A comparison of various normal-mode initialization schemes and the inclusion of diabatic processes. *Tellus*, **40A**, 1-25.

Fiorino, M and T.T. Warner, 1981: Incorporating surface winds and rainfall rates into the initialization of a mesoscale hurricane model. *Mon. Wea. Rev.*, **109**, 1914-1929.

Hartnett, E., G. Forbes and R. Hadlock, 1989: ERICA Experiment on Rapidly Intensifying Cyclones over the Atlantic: Field Phase Summary. Available from ERICA Data Center, Drexal University.

Heckley, A. H., G. Kelly, and M. Tiedtke, 1990: On the use of satellite-derived heating rates for data assimilation within the tropics. *Mon. Wea. Rev.*, **118**, 1743-1757.

Hoke, J. E. R. A. Anthes, 1976: The initialization of numerical models by a dynamical initialization technique. *Mon. Wea. Rev.*, **104**, 1551-1556.

Kasahara, A., A. Mizzi, and L. J. Donner, 1992: Impact of cumulus initialization on the spinup of precipitation forecasts in the tropics. *Mon. Wea. Rev.*, **120**, 1360-1380.

Kessler, E., 1974: Model of precipitation and vertical air currents. *Tellus*, **26**, 519-542.

Krishnamurti, T. N., K. Ingles, S. Cocke, R. Pasch, and T. Kitade, 1984: Details of low latitude medium range weather prediction using a global spectral model II. Effect of orography and physical initialization. *J Meteor. Soc. Japan*, **62**, 613-649.

Kurihara, Y. and R. E. Tuleya, 1981: A numerical simulation study on the genesis of a tropical storm. *Mon. Wea. Rev.*, **109**, 1629-1653.

Kuo, H. L. and W. H. Raymond, 1980: A quasi-one-dimensional cumulus cloud model and parameterization of cumulus heating and mixing effects. *Mon. Wea. Rev.*, **108**, 991-1009

Lejenas, H., 1980: On the influence of the technique of nonlinear normal mode initialization on the nonconvective precipitation rate. *Mon. Wea. Rev.*, **108**, 1465-1468.

Leslie, L. M., G. A. Mills, L. W. Logan, D. J. Gauntlett, G. A. Kelly, J. L. McGregor and M. J. Manton, 1985: A high resolution primitive equation NWP model for operations and research. *Aust. Meteor. Mag.*, **33**, 11-35.

Liu, J. Y. and H. D. Orville, 1969: Numerical modeling of precipitation and cloud shadow effects on mountain- induced cumuli. *J. Atmos. Sci.*, **26**, 1283-1298.

Martin, D. W., B. M. Goodman, T. J. Schmit and E. C. Cutrine, 1990: Estimates of daily rainfall over the Amazon basin. *J. G. R.*, **95**, 17043-17050.

Mathur, M. B., H. S. Bedi, T. N. Krishnamurti, M. Kanamitsu and J. S. Woollen, 1992: Use of satellite-derived rainfall for improving tropical forecasts. *Mon. Wea. Rev.*, **120**, 2540-2560.

McGregor, J. L., L. M. Leslie and D. J. Gauntlett, 1978: The ANMRC limited-area model: consolidated formulation and operational results. *Mon. Wea. Rev.*, **106**, 427-438.

Mills, G. A. and R. S. Seaman, 1990: The BMRC regional data assimilation system. *Mon. Wea. Rev.*, **118**, 1217-1237.

Mizzi, A., P., and A. Kasahara, 1989: Intercomparison of daily values of atmospheric variables, including diabatic heating rates, from the ECMWF, GFDL and Goddard Laboratory for Atmospheres FGGE level IIIb analyses. *J. Geophys. Res.*, **44**, 14717-14748.

Olson, William S., 1993: Physical retrieval of precipitation water contents from special sensor microwave/Imager (SSM/I) Data-Part II: Retrieval method and applications. To be submitted to *J. Appl. Meteor.*

Perkey, D. J., 1976: A description of preliminary results from a fine-mesh model for forecasting quantitative precipitation. *Mon. Wea. Rev.*, **104**, 1513-1526.

Puri, K., and M. J. Miller, 1990: The use of satellite data in the specification of convective heating for diabatic initialization and moisture adjustment in numerical weather prediction models. *Mon.Wea. Rev.*, **118**, 67-93.

Raymond, W. H., 1988: High-order low-pass implicit tangent filters for use in finite area calculations. *Mon. Wea. Rev.*, **116**, 2132-2141.

_____, 1989: Theoretical investigation of spiral features in mesolow circulations. *Polar and Arctic Lows*, Editors P. F. Twitchell, E. A. Rasmussen and K. L. Davidson, DEEPAK Publishing, 191-200.

_____, 1993: Moist wind relationships. *Mon. Wea. Rev.*, **121**, 1992-2003.

Salmon, E. M., and T. T. Warner, 1986: Short-term numerical precipitation forecasts initialized using a diagnosed divergent-wind component. *Mon. Wea. Rev.*, **114**, 2122-2132.

Schlesinger, R. E., 1990: Feedback of deep moist convection to its near environment as diagnosed from three-dimensional numerical model output: Results from an early experiment. *J. Atmos. Sci.*, **47**, 1390-1412.

Schubert, W. H. and J. J. Hack, 1982: Inertial stability and tropical cyclone development. *J. Atmos. Sci.*, **39**, 1687-1697.

Shapiro, L. J., and D. E. Stevens, 1980: Parameterization of convective effects on the momentum and vorticity budgets of synoptic-scale Atlantic tropical waves. *Mon. Wea. Rev.*, **108**, 1816-1826.

Sundqvist, H., E. Berge and J. E. Kristjansson, 1989: Condensation and cloud parameterization studies with a mesoscale numerical weather prediction model. *Mon. Wea. Rev.*, **117**, 1641-1657.

Tarbell, T. C., T. T. Warner and R. A. Anthes, 1981: An example of the initialization of the divergent wind component in a mesoscale numerical weather prediction model. *Mon. Wea. Rev.*, **109**, 77-95.

Turpeinen, O. M., L. Garand, R. Benoit and M. Roch, 1990: Diabatic initialization of the Canadian regional finite-element (RFE) model using satellite data. Part I: Methodology and application to a winter storm. *Mon. Wea. Rev.*, **118**, 1381-1395.

Wallace, J. M. and P. V. Hobbs, 1977: *Atmospheric Science, An Introductory Survey.* Academic Press, New York, 467pp.

Wang, W. and T. T. Warner, 1988: Use of four-dimensional data assimilation by newtonian relaxation and latent-heat forcing to improve a mesoscale-model precipitation forecast: A case study. *Mon. Wea. Rev.*, **116**, 2593-2613.

Wergen, W., 1988: The diabatic ECMWF normal mode initialization scheme. *Beitr. Phys. Atmosph.*, **61**, 274-302.

Wolcott, S. W., and T. T. Warner: 1981: A humidity initialization utilizing surface and satellite data. *Mon. Wea. Rev.*, **109**, 1989-1998.

List of Figures

Fig. 12 Height field from the twenty four hour forecast with diabatic forcing DF(0.25) inserted gently at time step 120 (hour 10) and removed gently by step 165 (hour 13.75). Contour interval is 4 m.

Fig. 13. Same as Fig. 12 but for vorticity. Contour interval is 4.0×10^{-5} s^{-1}.

Fig. 14 Same as Fig. 12 but for divergence. Contour interval is 1.0×10^{-5} s^{-1}.

Fig. 15 Bar graph of maximum rainfall as a function of the diabatic forcing. Control case contains no rainfall in the vicinity of Emily but does have significant rainfall over elevated regions.

Fig. 16 Total rainfall is shown for two cases having different diabatic forcing in the vertical. Dashed lines are associated with lower level forcing while the elevated forcing gives the solid line. Contour interval is 4 cm.

Fig. 17 The number of grid scale condensations are shown as a function of the diabatic forcing which varies in its vertical distribution or magnitude.

Fig. 18 Shown is the integrated rain water (kg m^{-2} x 10) from the fourteen hour forecast.

Fig. 19 Retrieved estimates of the integrated precipitating liquid and ice from SSM/I radiances (Olson, 1993).

Fig. 20 Presented are the omega distributions in the adiabatic (top) and diabatic (bottom) initialized fields associated with ERICA IOP-5. Left-hand panels show the 700 mb distributions, while the right-hand panels give the 400 mb distribution.

Fig. 21 Presented are the 500 mb wind speed from the twenty four hour (control) forecast (upper left), twelve hour forecast with adiabatic initial conditions (upper right), twelve hour forecast with 2 hours of diabatic forcing (lower left), and twelve hour forecast with 4 hours of diabatic forcing (lower right).

Fig. 22 Same as in Fig 21 but for the 700 mb mixing ratio.

Fig. 23 Same as in Fig 21 but showing the rainfall.

Fig. 24 Shown is the grid averaged precipitation rate (mm h^{-1}) during a twenty four hour period ending at 1200 UTC 20 Jan 1988. The grid scale calculations with no clouds are labeled large scale while explicit cloud calculations, with and without a diabatic initialization and initialized cloud and rain water, can be compared against estimates of the hourly precipitation rate obtained from satellite infrared image cloud-top temperatures.

Fig. 25 Mean sea level pressure from a 12 h forecast beginning with a diabatic initialization. Contour interval is 4 mb.

Fig. 26 Mean sea level from a 12 h forecast that uses diabatic initialization and diabatic forcing. Contour interval is 4 mb.

Fig. 27 The vertically integrated cloud water (x 100 kg m^{-2}) at 1200 UTC 22 April 1988 from a 12 hour forecast initialized with cloud and rain water from the 12 hour preforecast. Contour interval is 3 .

Fig. 28 The response in the grid scale condensations, as a function of vertical modes, to changes in the magnitude of the diabatic initialization.

Fig. 29 Shown is the average precipitation per time step, using in the assimilation the model generated (MG) fields from the preforecast, with and without the cumulus parameterization scheme and the surface and upper air data.

Fig. 30 The number of grid scale condensations are shown as a function of cloud water (Cl), rain water (Rn), diabatic initialization (DI) and whether the model generated fields (MG) or global fields are used in the assimilation process.

Fig. 31 Same as Fig. 30 but showing the average precipitation rate.

Fig. 32 The per cent of the total cloud water at each vertical level at the end of a 12 h forecast is shown for two forecasts that have different amounts of data in the initialization.

Fig. 33 Same as Fig. 32 but for total rain water.

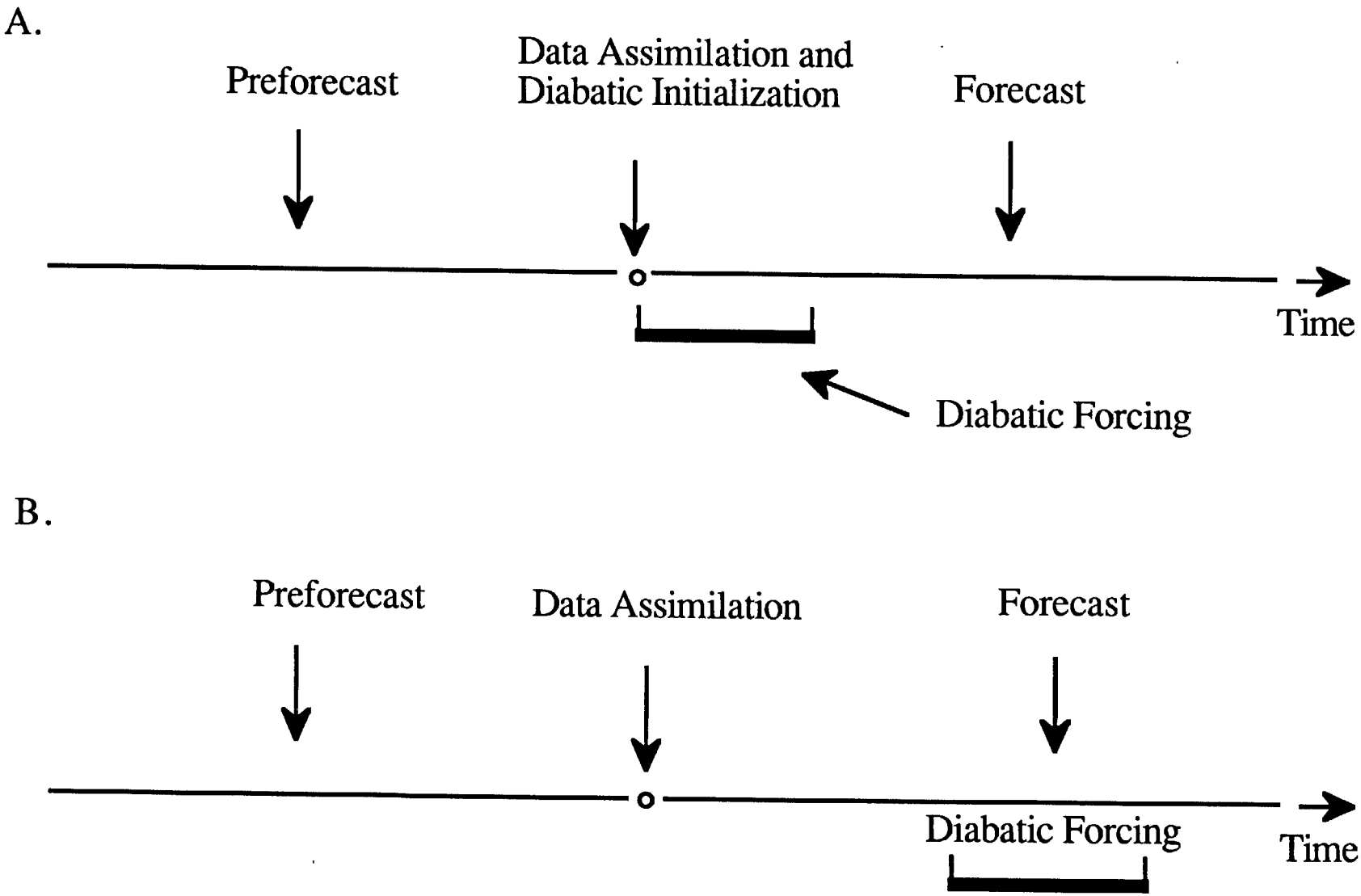
A.
Preforecast
Data Assimilation and
Diabatic Initialization
Forecast
Time
Diabatic Forcing
B.
Preforecast
Data Assimilation
Forecast
Diabatic Forcing
Time

Fig. 1

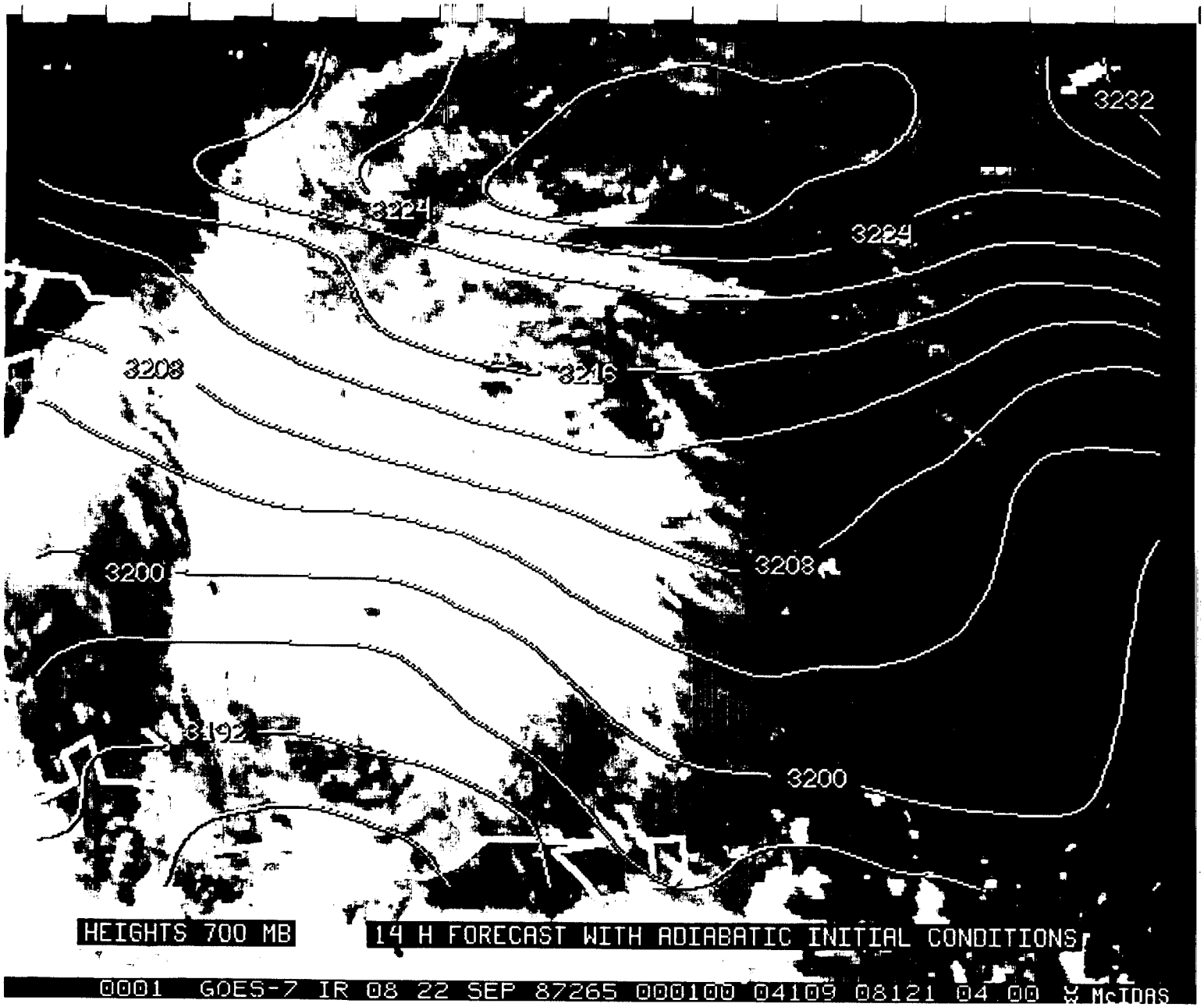
3232
3224
3224
3216
3208
3208
3200
3192
3200
HEIGHTS 700 MB
14 H FORECAST WITH ADIABATIC INITIAL CONDITIONS
0001 GOES-7 IR 08 22 SEP 87265 000100 04109 08121 04 00 McIDAS

Fig 2

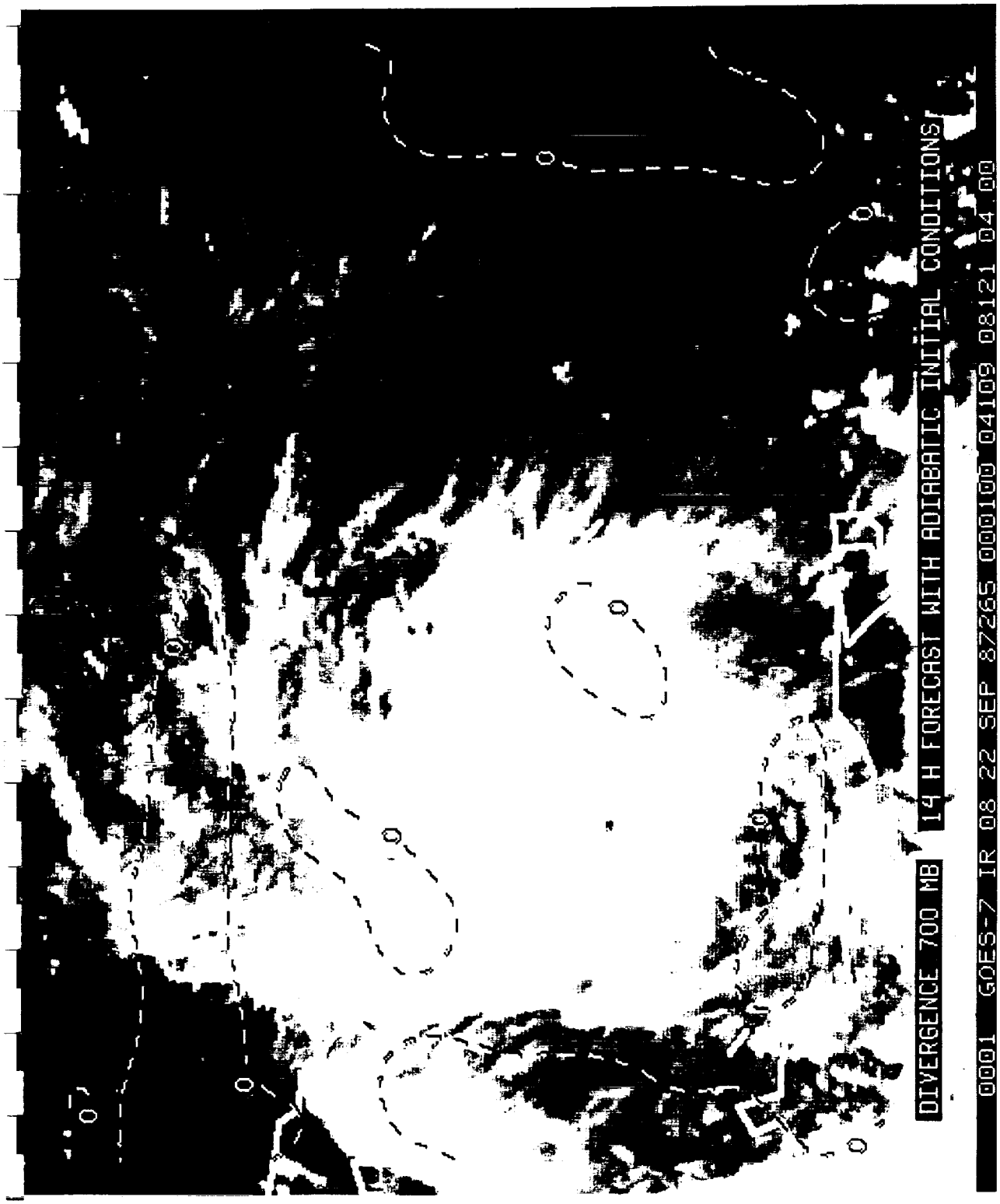
DIVERGENCE 700 MB
14 H FORECAST WITH ADIABATIC INITIAL CONDITIONS
0001 GOES-7 IR 08 22 SEP 87265 000100 04109 08121 04 00

Fig 3

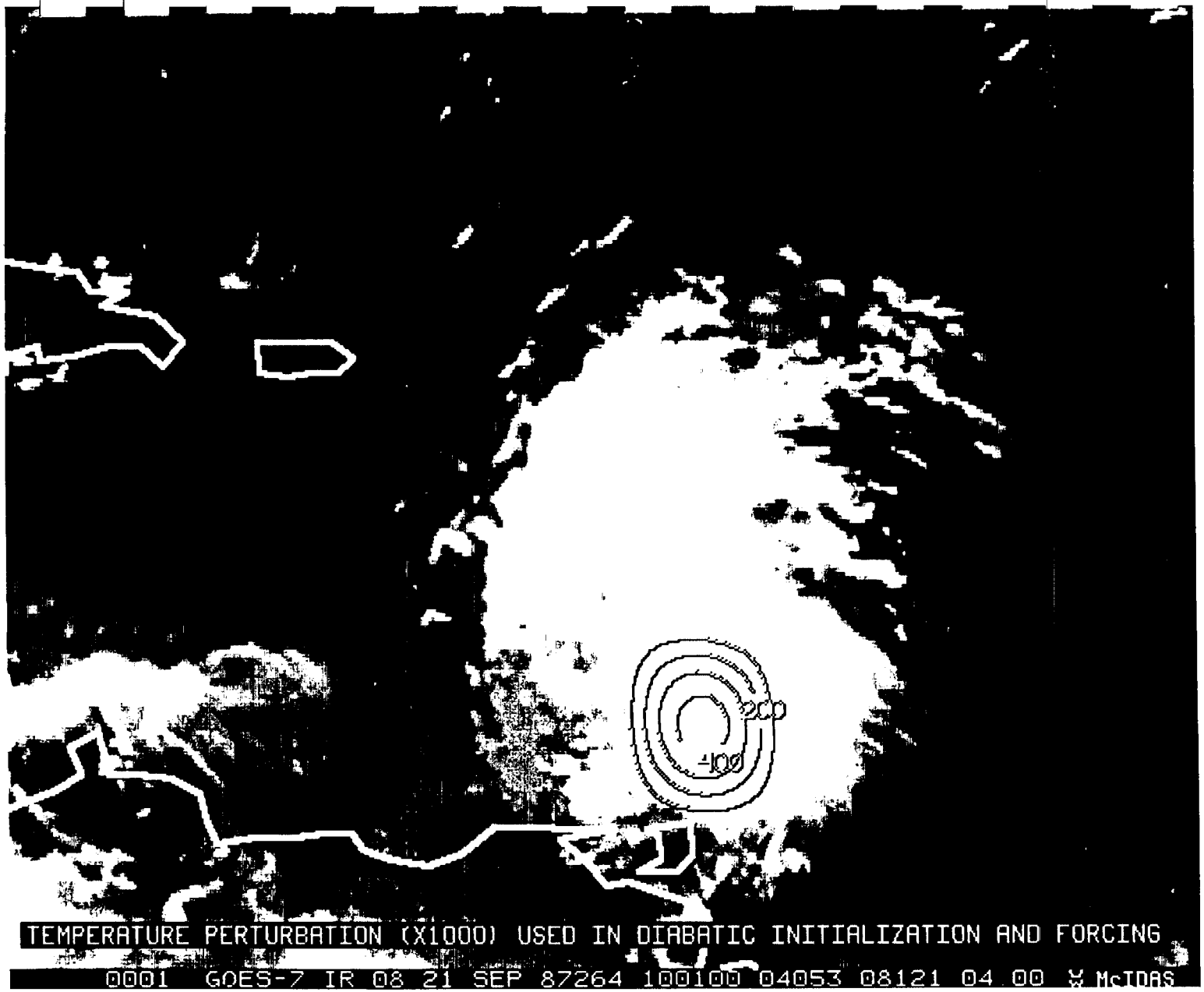
TEMPERATURE PERTURBATION (X1000) USED IN DIABATIC INITIALIZATION AND FORCING
0001 GOES-7 IR 08 21 SEP 87264 100100 04053 08121 04 00 McIDAS

Fig 4

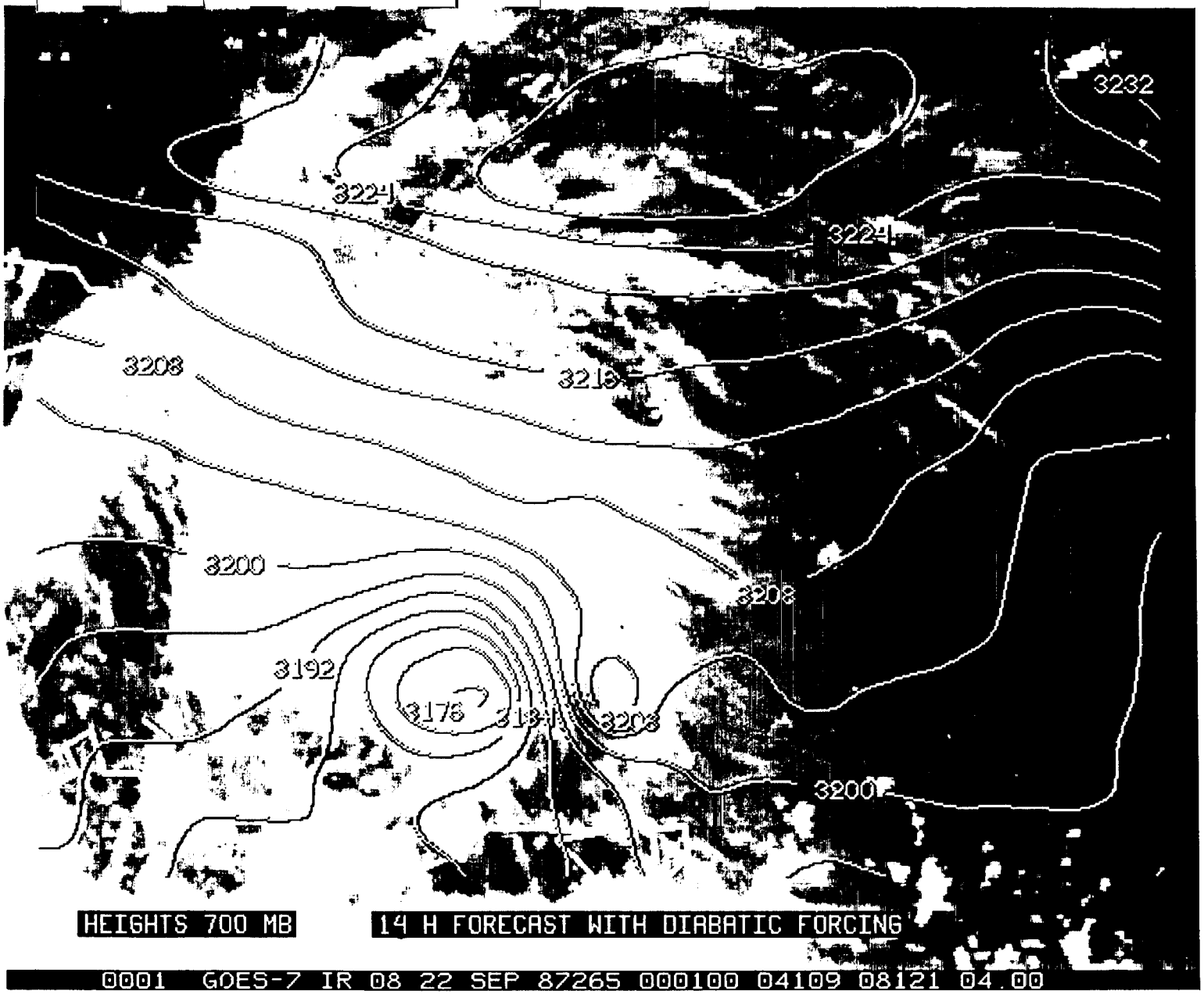
3232
3224
3224
3208
3216
3200
3208
3192
3176
3184
3208
3200
HEIGHTS 700 MB
14 H FORECAST WITH DIABATIC FORCING
0001 GOES-7 IR 08 22 SEP 87265 000100 04109 08121 04.00

Fig 5

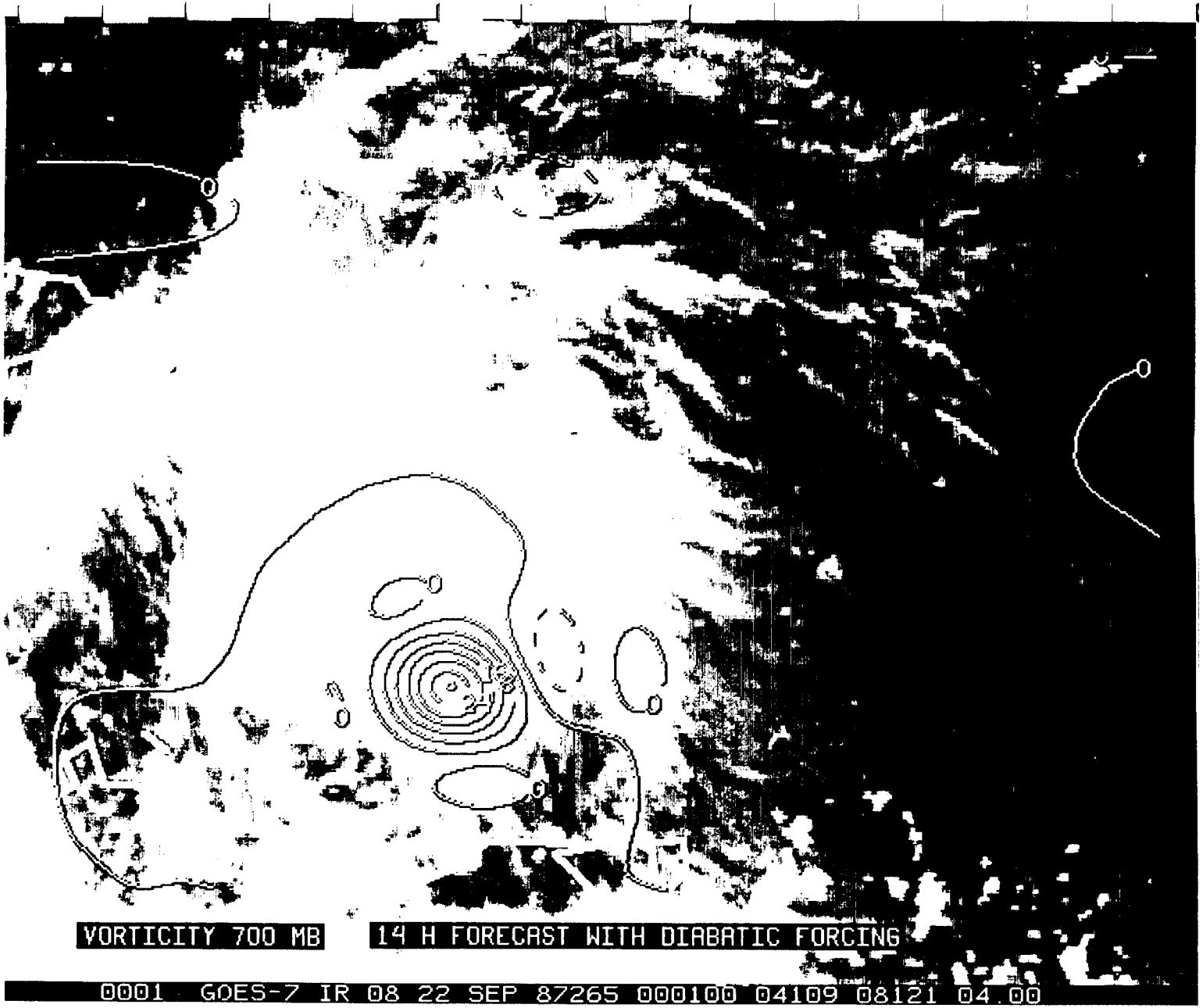
VORTICITY 700 MB
14 H FORECAST WITH DIABATIC FORCING
0001 GOES-7 IR 08 22 SEP 87265 000100 04109 08121 04.00

Fig 1

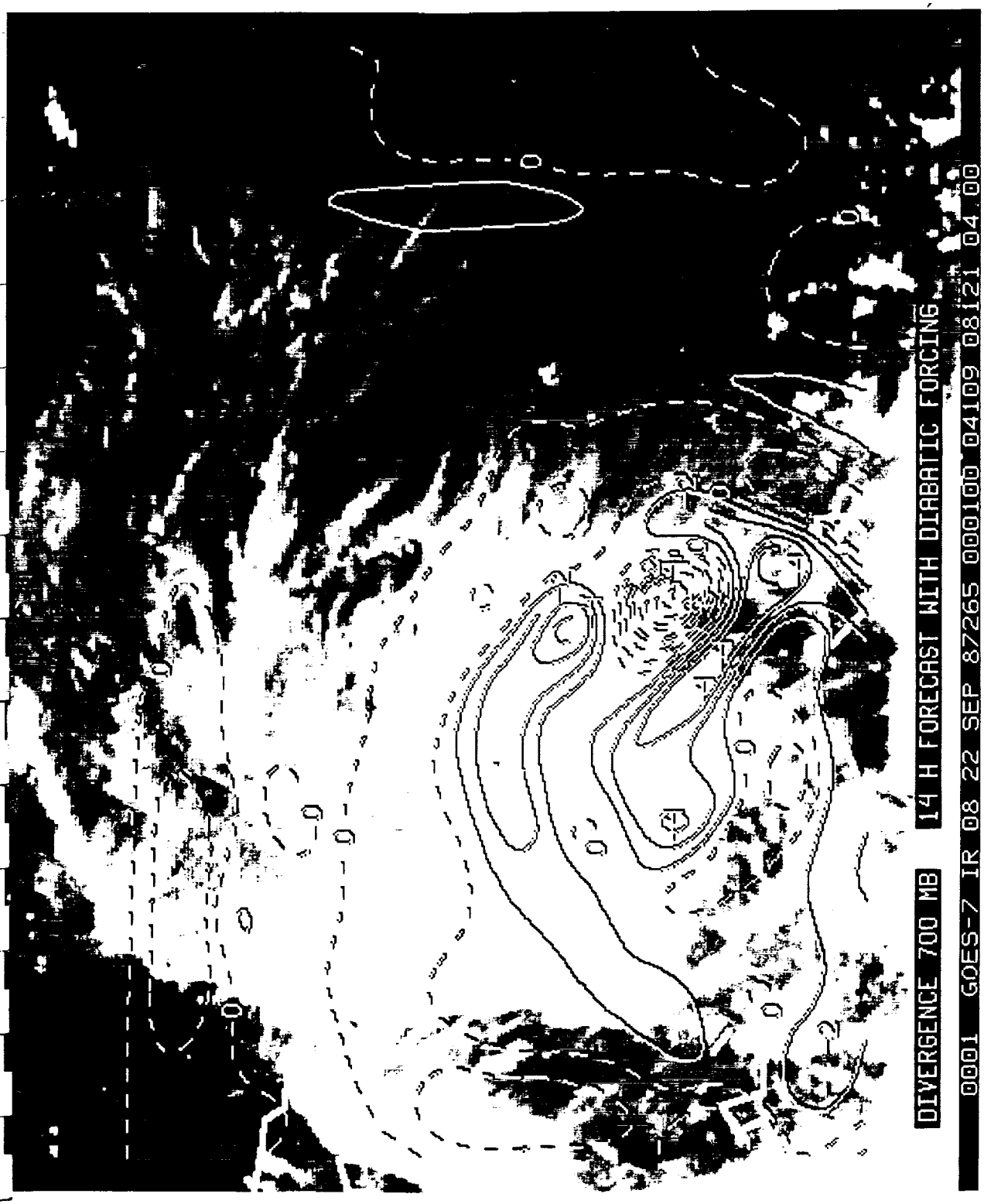
DIVERGENCE 700 MB
14 H FORECAST WITH DIABATIC FORCING
0001 GOES-7 IR 08 22 SEP 87265 000100 04109 08121 04 00

Fig 7

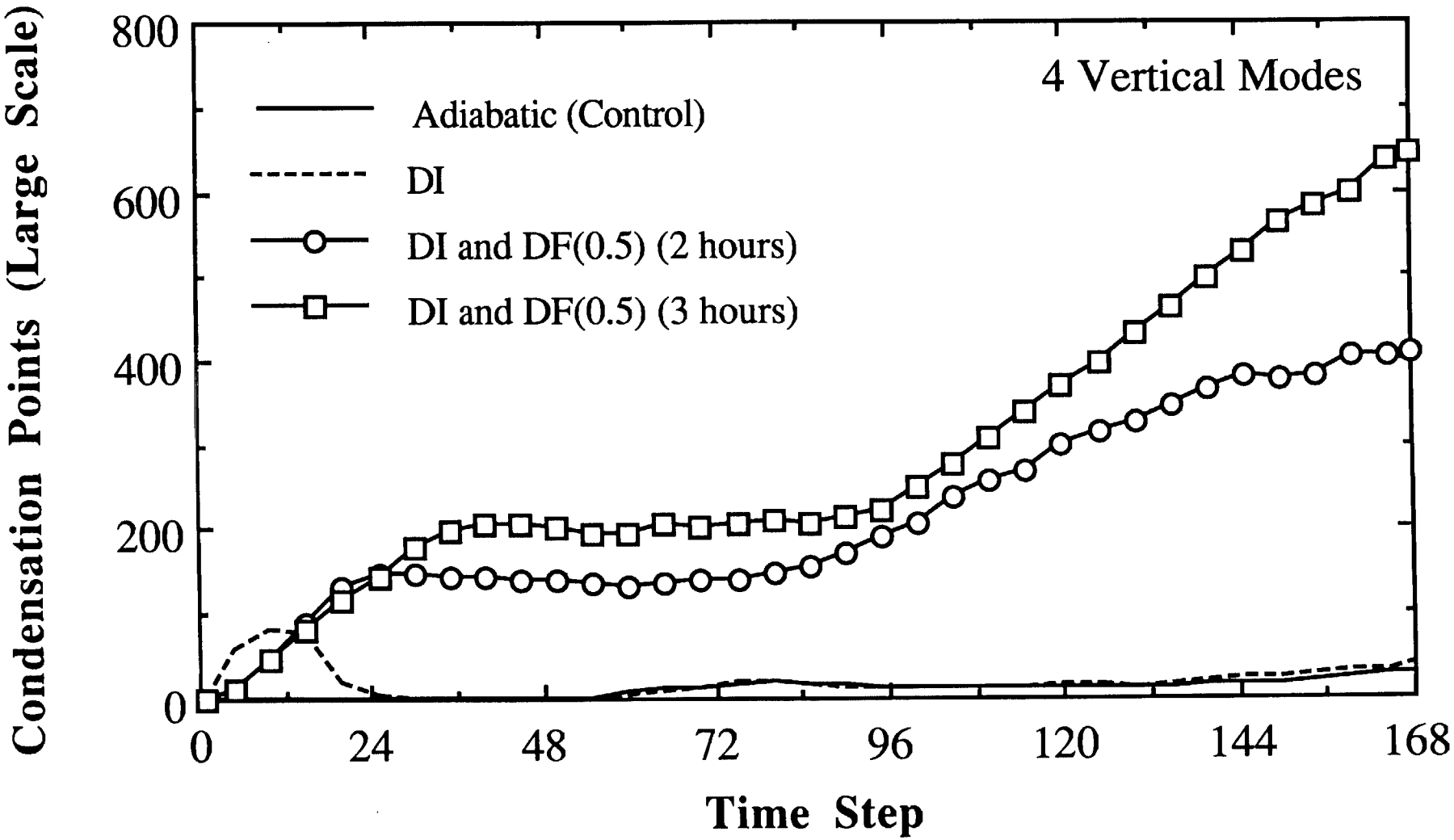
4 Vertical Modes
Adiabatic (Control)
DI
DI and DF(0.5) (2 hours)
DI and DF(0.5) (3 hours)
Condensation Points (Large Scale)
800
600
400
200
0
0
24
48
72
96
120
144
168
Time Step

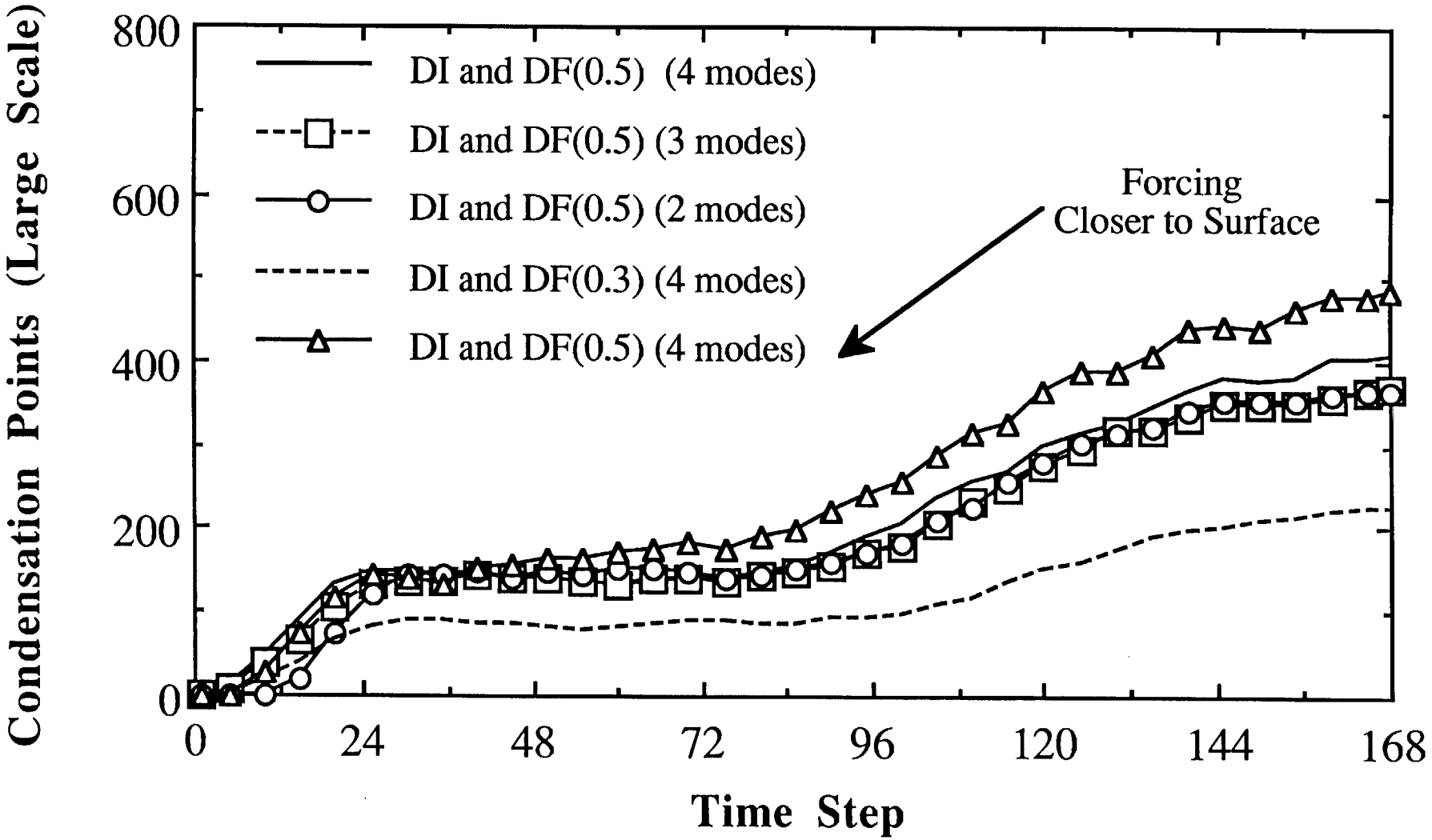
Condensation Points (Large Scale)
800
600
400
200
0
0
24
48
72
96
120
144
168
Time Step
DI and DF(0.5) (4 modes)
DI and DF(0.5) (3 modes)
DI and DF(0.5) (2 modes)
DI and DF(0.3) (4 modes)
DI and DF(0.5) (4 modes)
Forcing
Closer to Surface

Fig 9

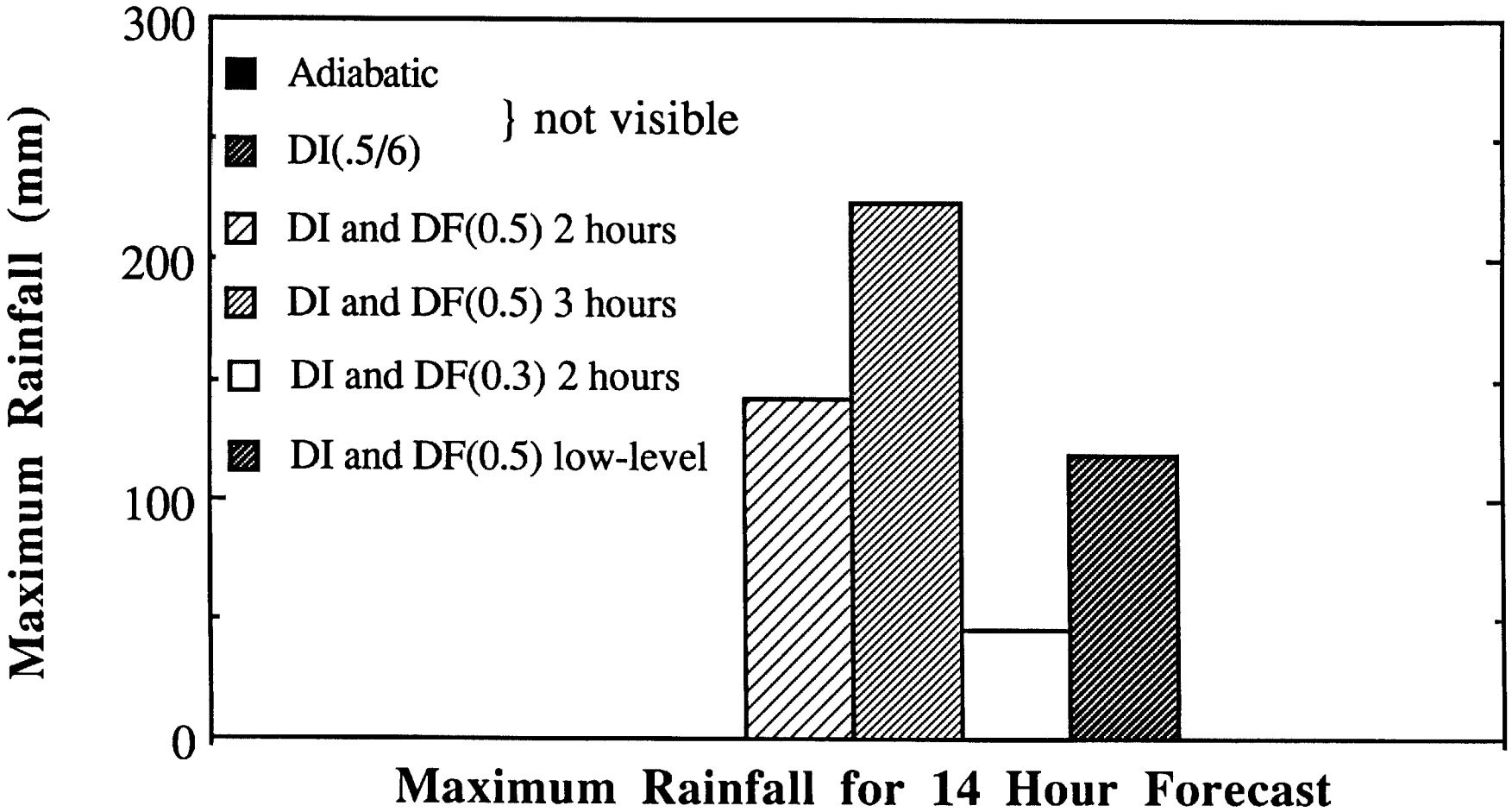
300
200
100
0
Maximum Rainfall (mm)
Adiabatic
DI(.5/6)
} not visible
DI and DF(0.5) 2 hours
DI and DF(0.5) 3 hours
DI and DF(0.3) 2 hours
DI and DF(0.5) low-level
Maximum Rainfall for 14 Hour Forecast

Fig 10

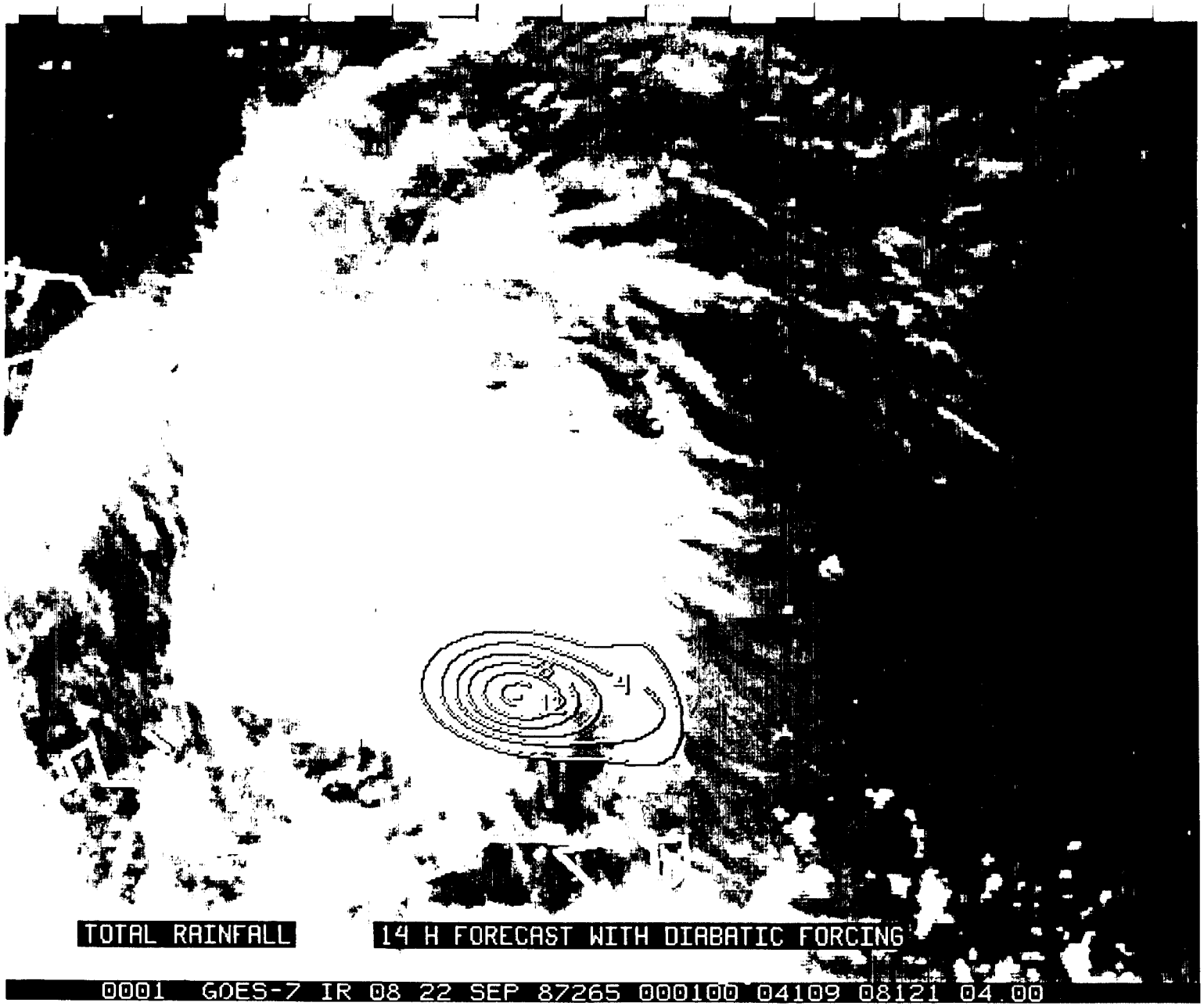
TOTAL RAINFALL
14 H FORECAST WITH DIABATIC FORCING
0001 GOES-7 IR 08 22 SEP 87265 000100 04109 08121 04.00

Fig 11

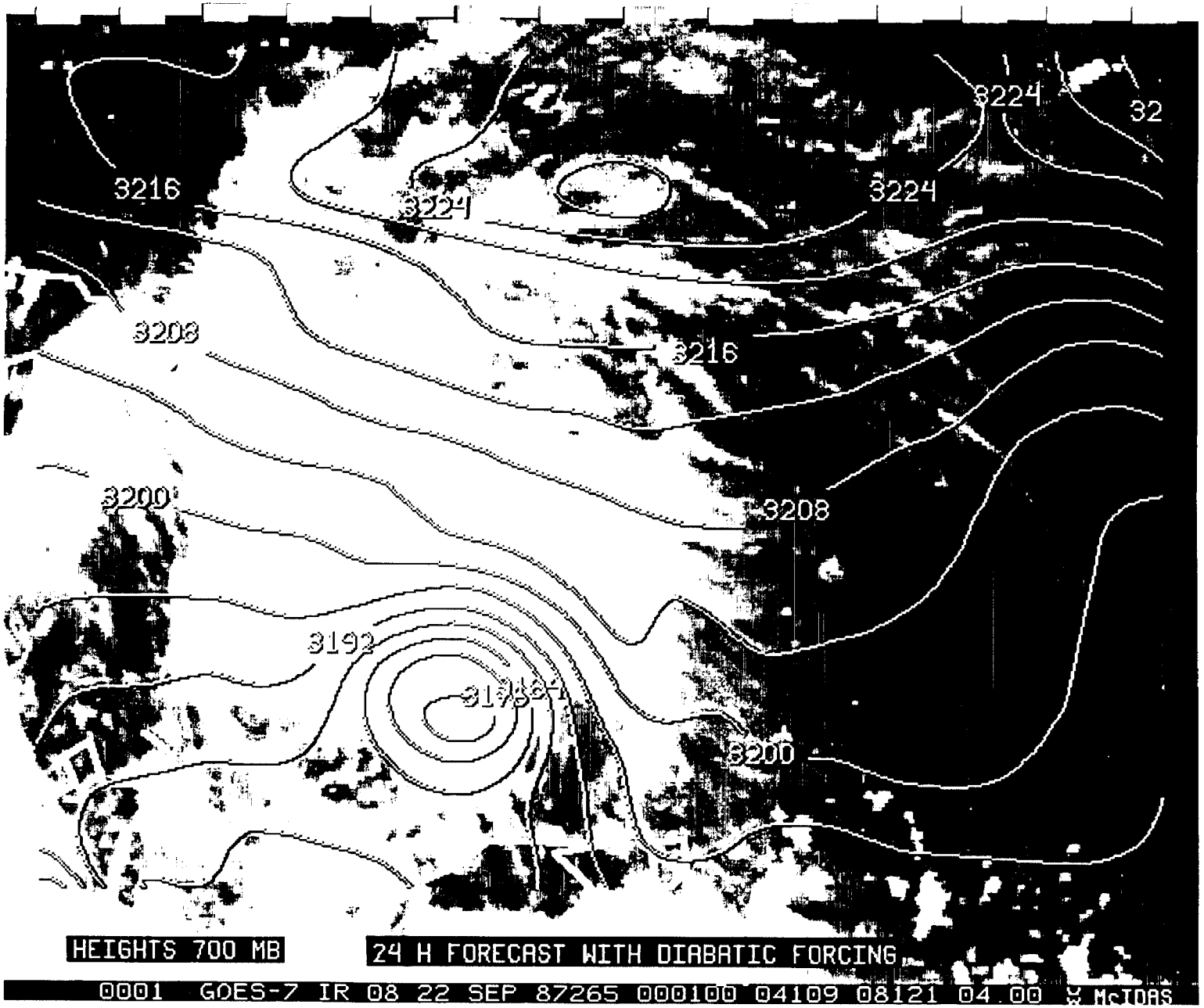
3224
32
3216
3224
3224
3208
3216
3200
3208
3192
3184
3200
HEIGHTS 700 MB
24 H FORECAST WITH DIABATIC FORCING
0001 GOES-7 IR 08 22 SEP 87265 000100 04109 08121 04.00 ※ McIDAS

Fig 12

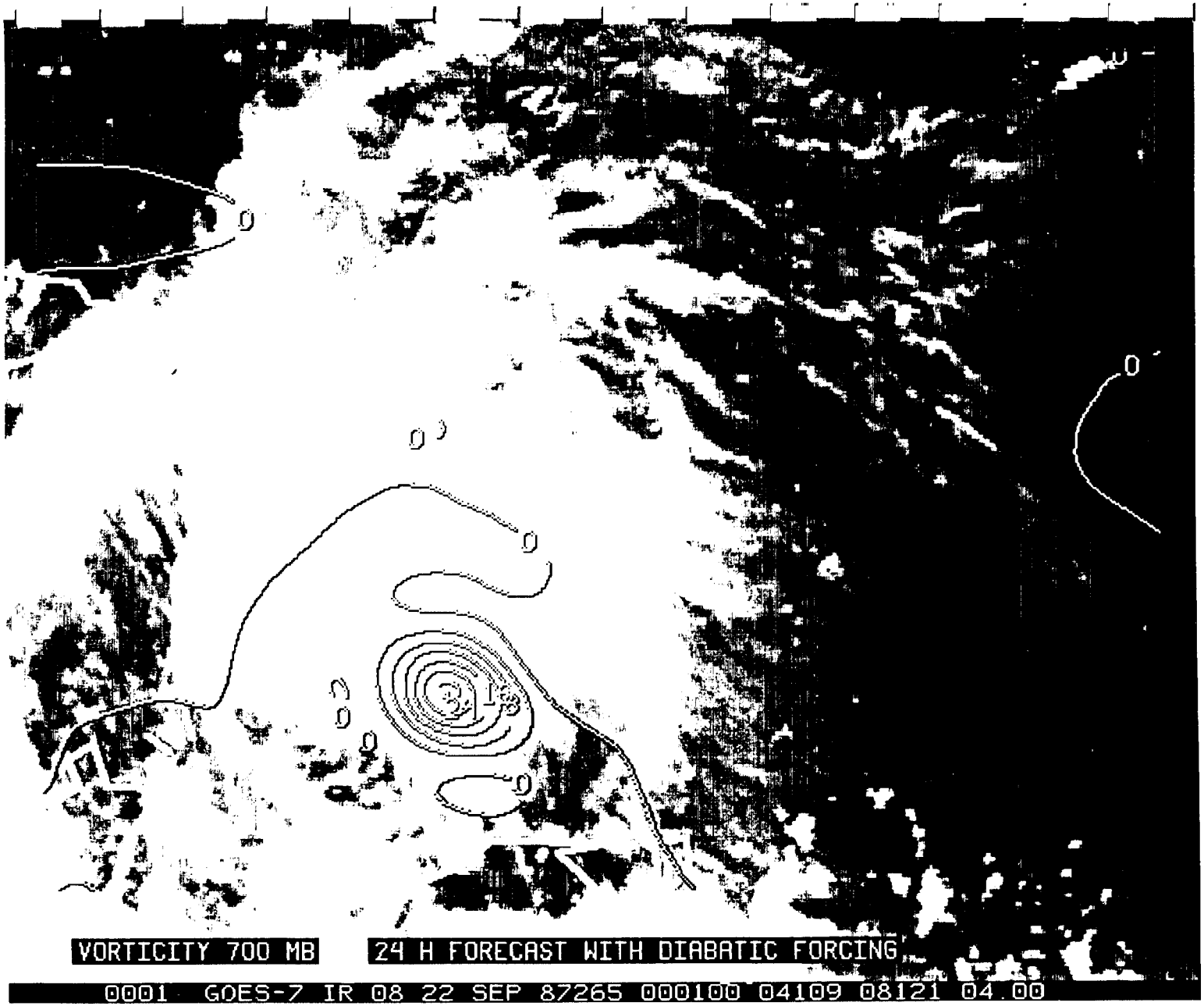
VORTICITY 700 MB
24 H FORECAST WITH DIABATIC FORCING
0001 GOES-7 IR 08 22 SEP 87265 000100 04109 08121 04 00

Fig 13

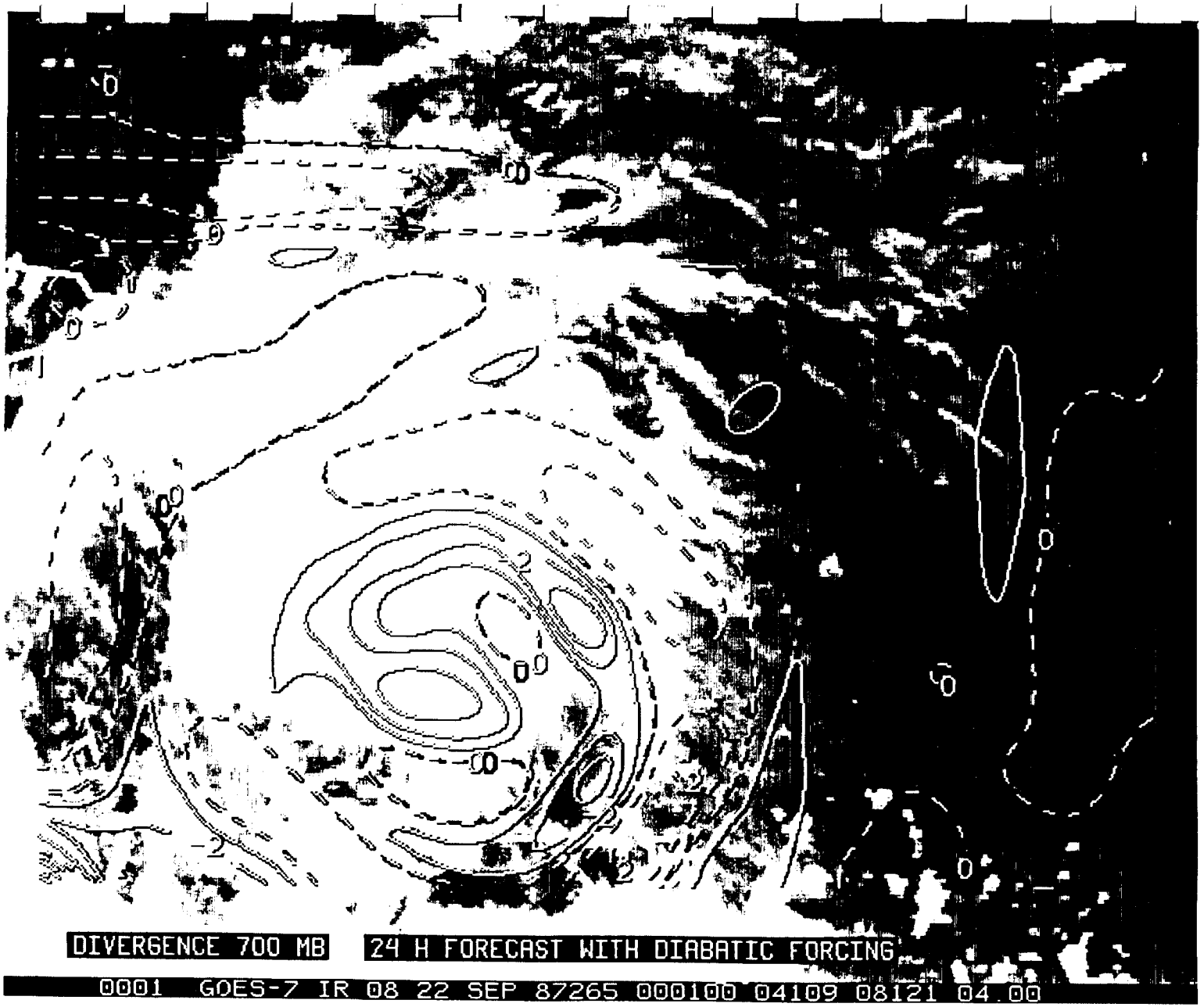
DIVERGENCE 700 MB
24 H FORECAST WITH DIABATIC FORCING
0001 GOES-7 IR 08 22 SEP 87265 000100 04109 08121 04 00

Fig 14

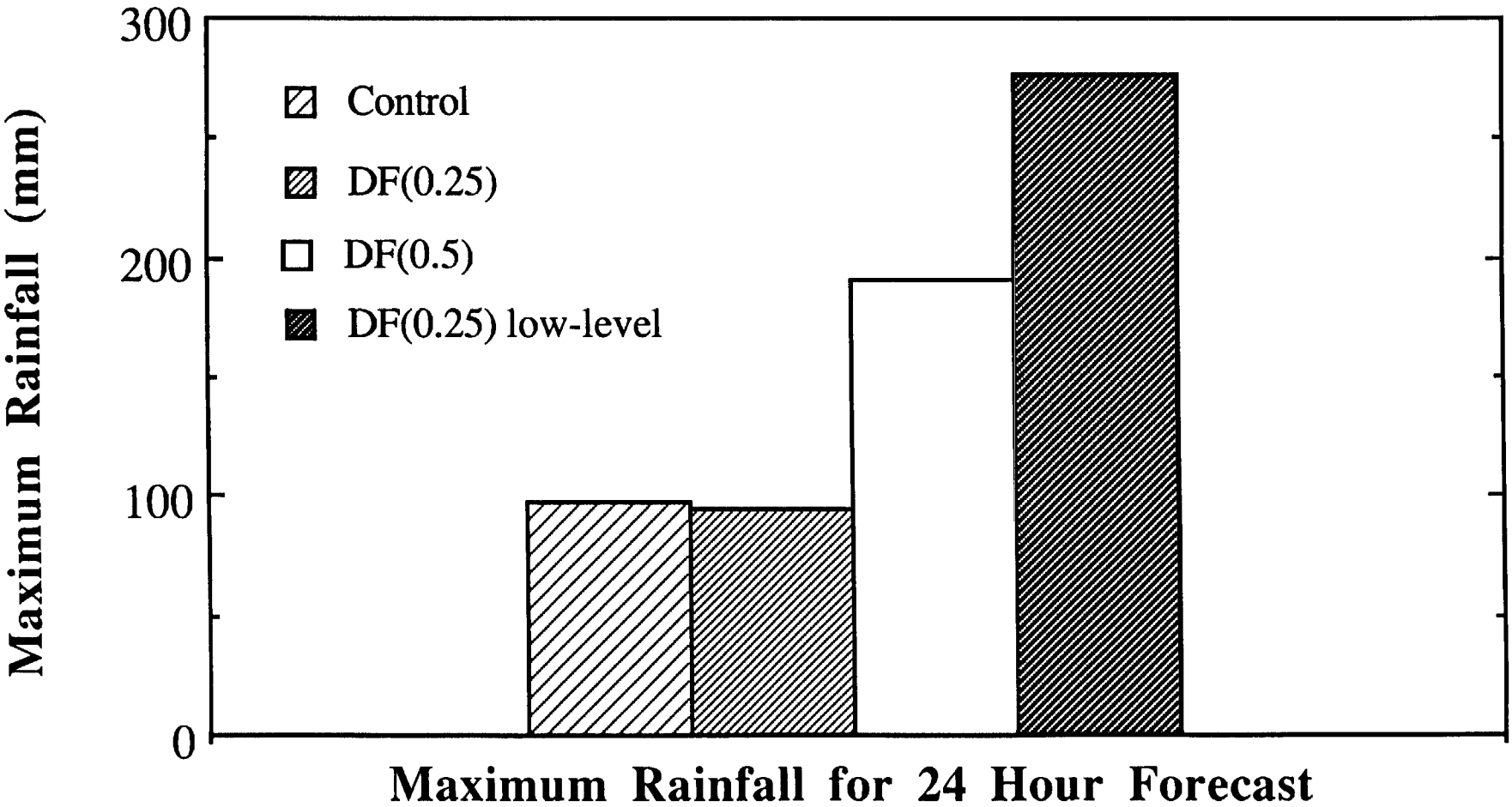
300
200
100
0
Maximum Rainfall (mm)
Control
DF(0.25)
DF(0.5)
DF(0.25) low-level
Maximum Rainfall for 24 Hour Forecast

Fig 15

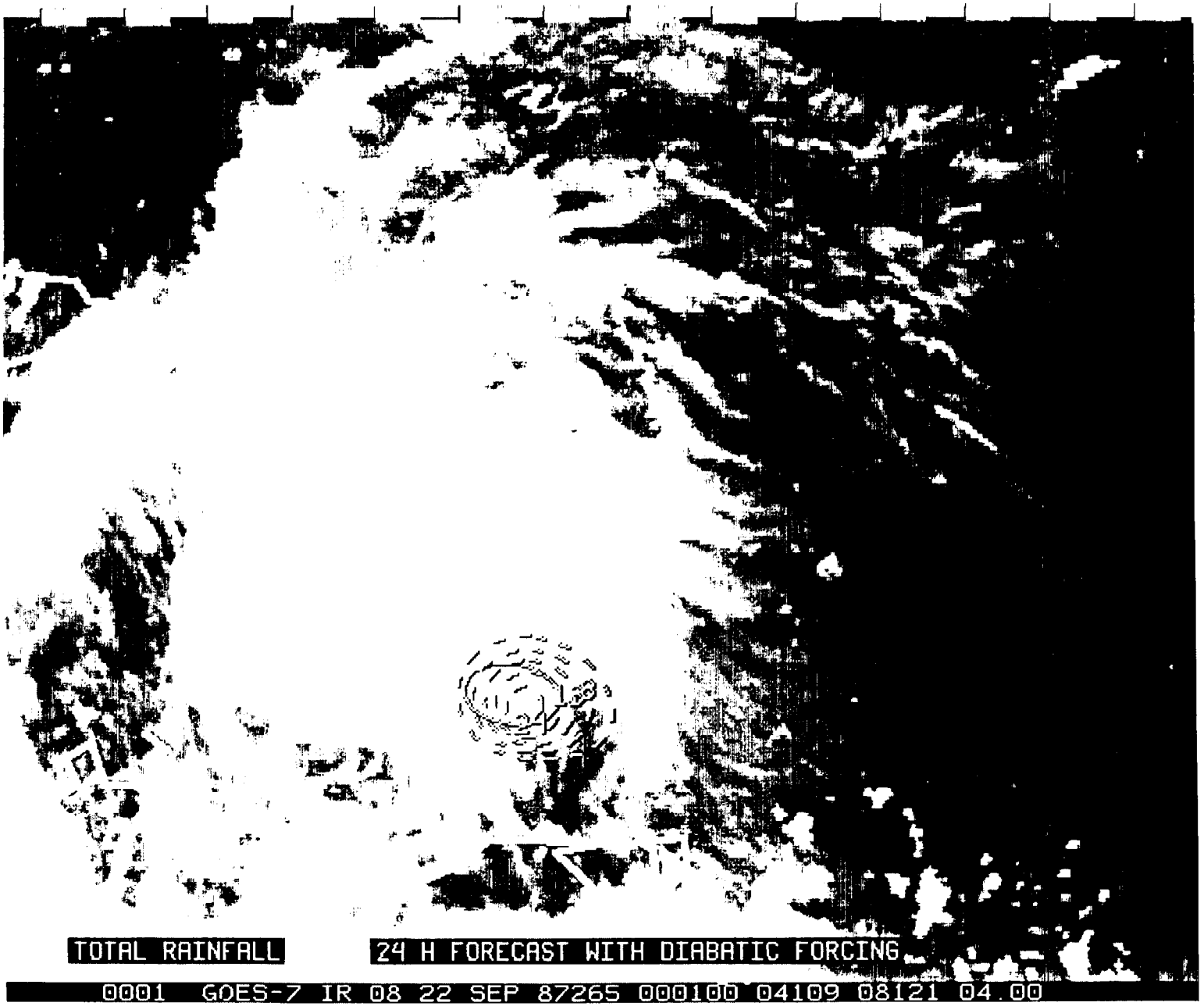
TOTAL RAINFALL
24 H FORECAST WITH DIABATIC FORCING
0001 GOES-7 IR 08 22 SEP 87265 000100 04109 08121 04.00

Fig 16

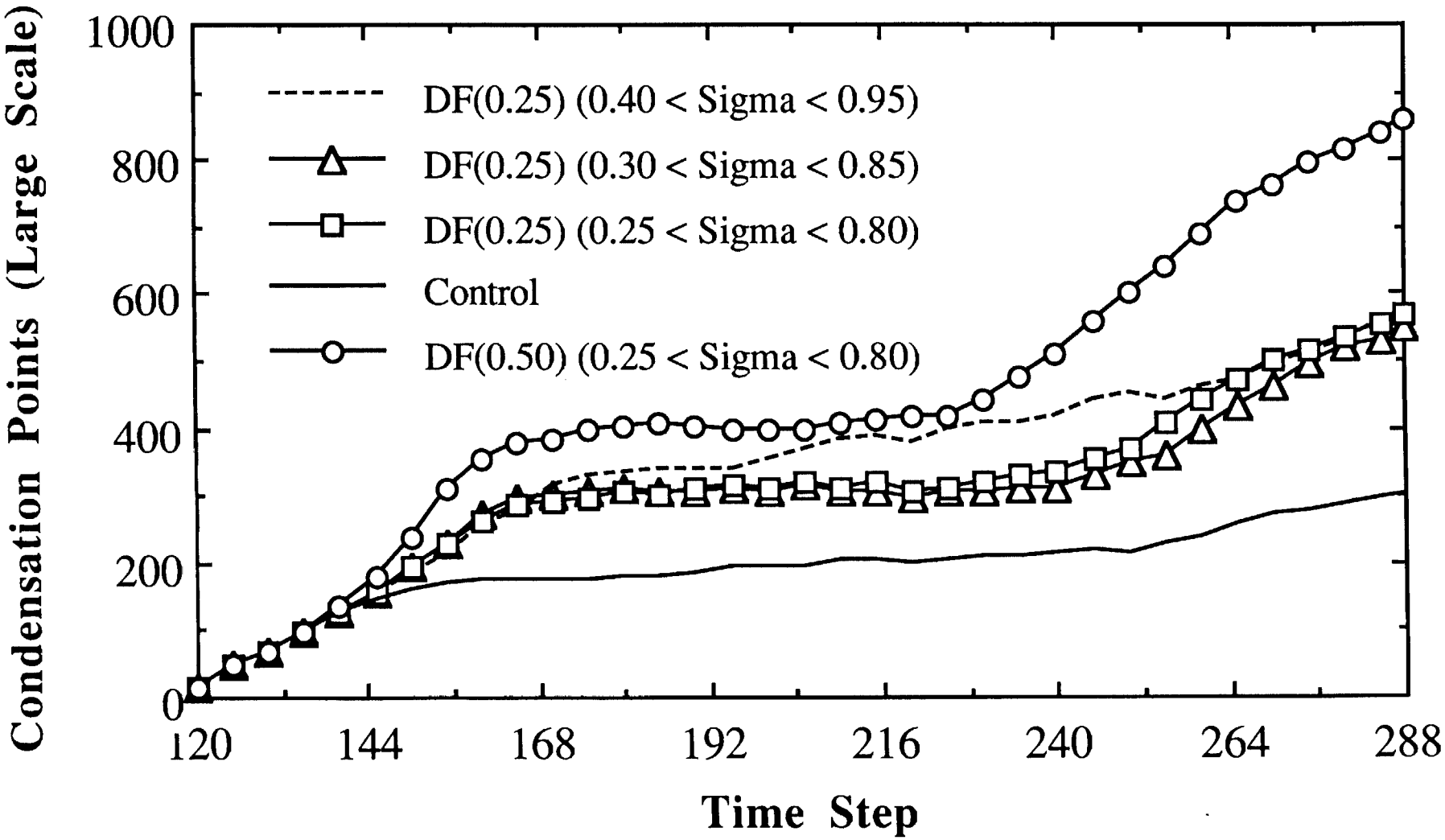
Condensation Points (Large Scale)
1000
800
600
400
200
0
120
144
168
192
216
240
264
288
Time Step
DF(0.25) (0.40 < Sigma < 0.95)
DF(0.25) (0.30 < Sigma < 0.85)
DF(0.25) (0.25 < Sigma < 0.80)
Control
DF(0.50) (0.25 < Sigma < 0.80)

Fig 17

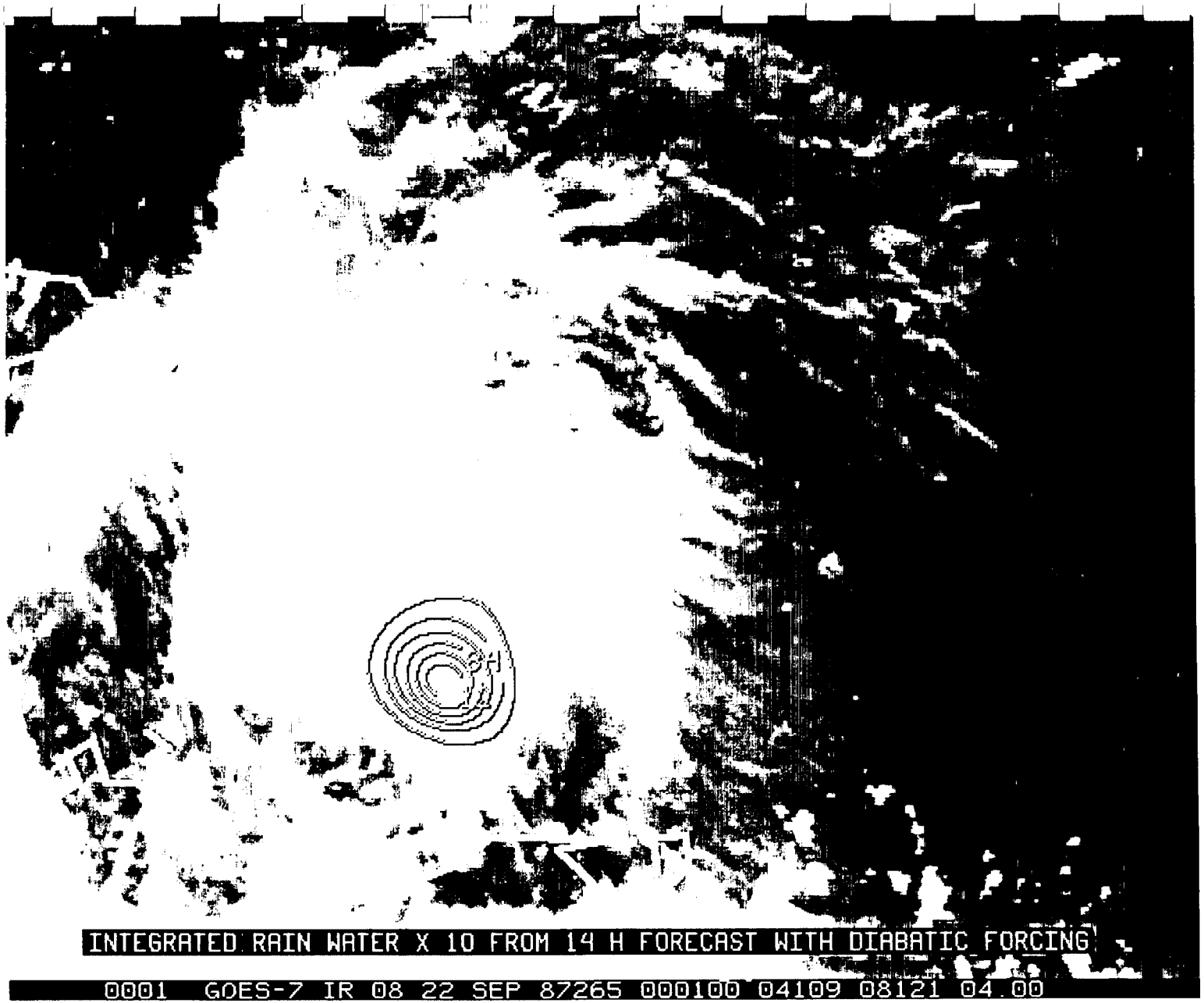
H
INTEGRATED RAIN WATER X 10 FROM 14 H FORECAST WITH DIABATIC FORCING
0001 GOES-7 IR 08 22 SEP 87265 000100 04109 08121 04.00

Fig 8

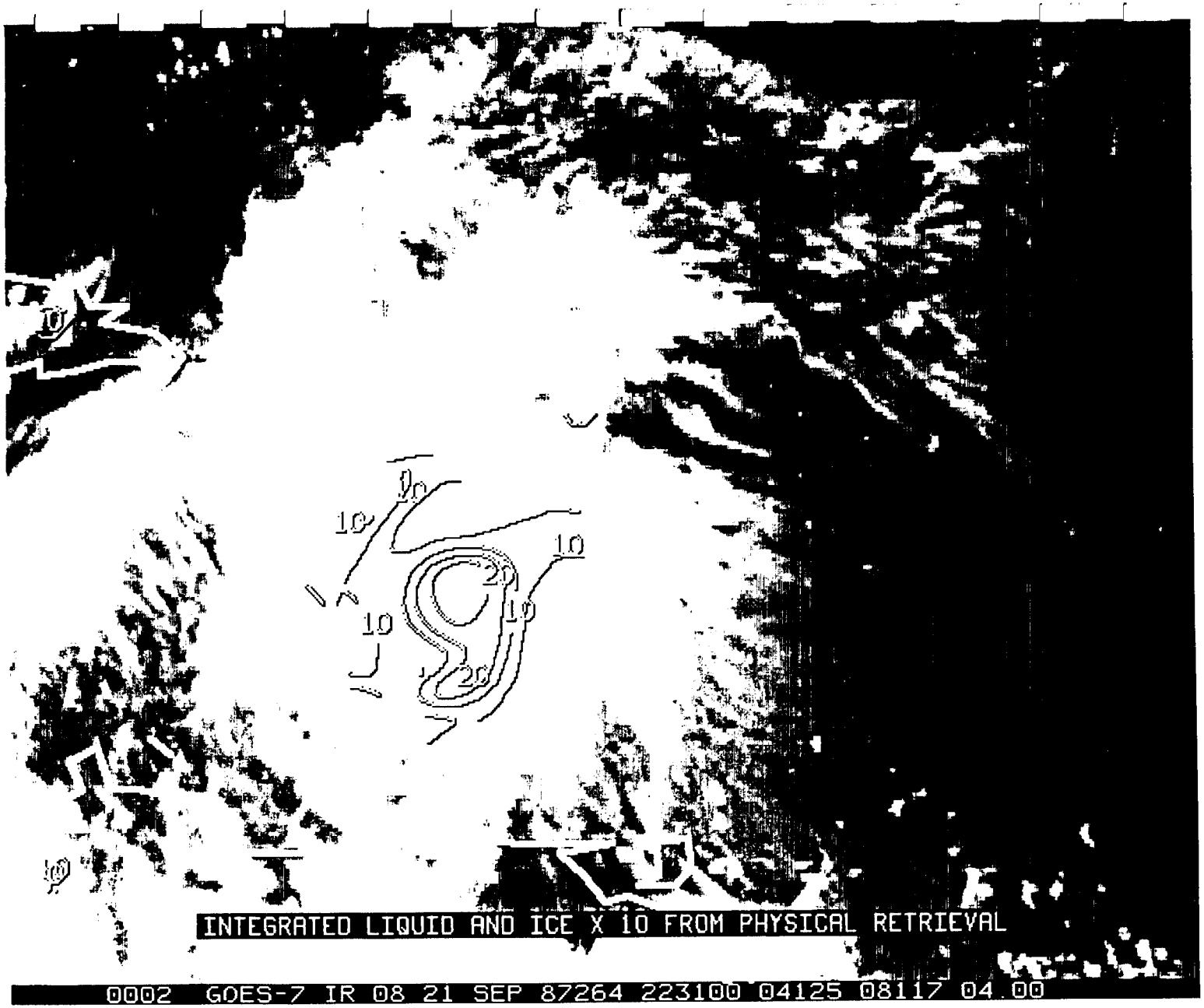
0
10
10
10
20
10
10
20
0
INTEGRATED LIQUID AND ICE X 10 FROM PHYSICAL RETRIEVAL
0002 GOES-7 IR 08 21 SEP 87264 223100 04125 08117 04.00

Fig 19

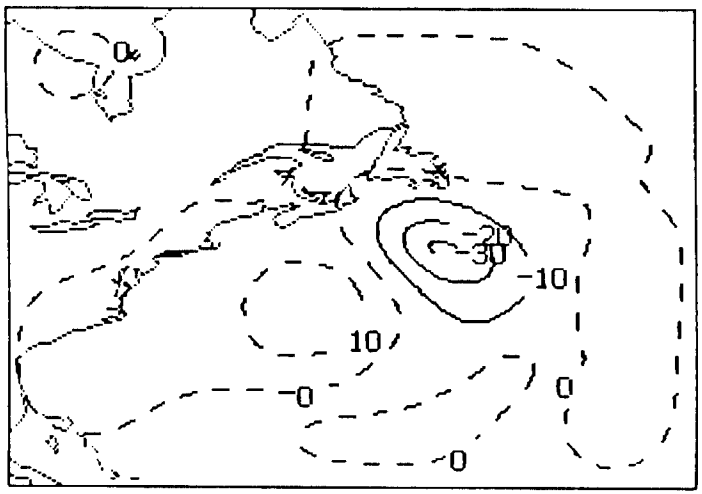

DMGP TIME 0. DAY 890120. 700. MB

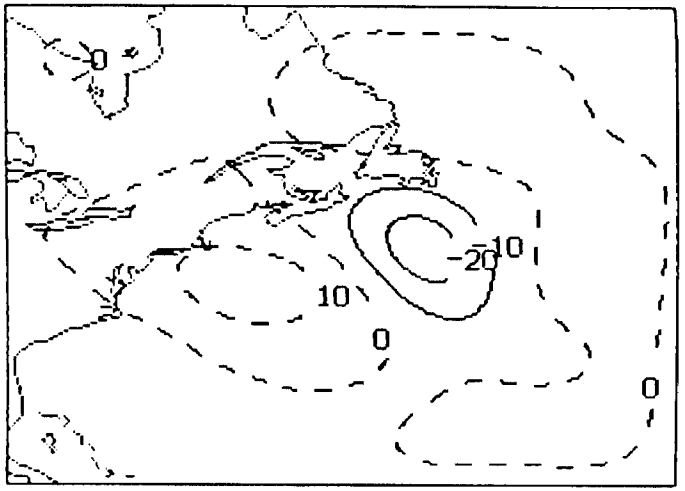

DMGP TIME 0. DAY 890120. 400. MB

ADIABATIC INITIALIZATION

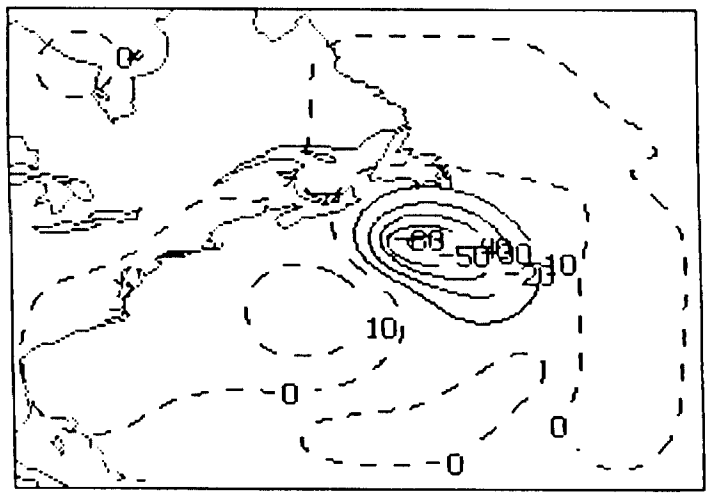

DMGP TIME 0. DAY 890120. 700. MB

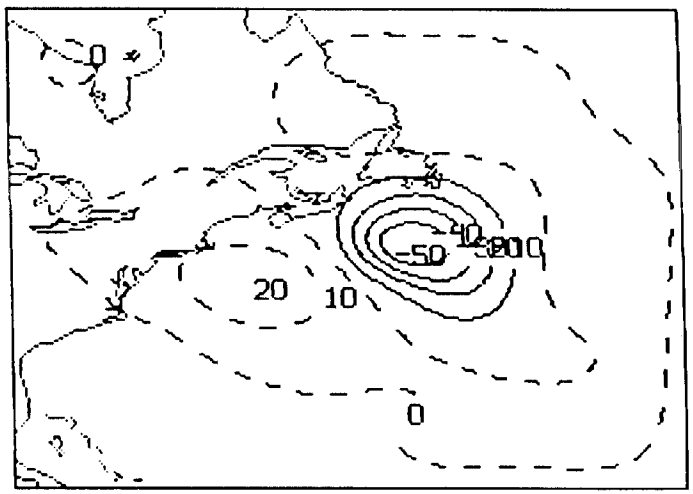

DMGP TIME 0. DAY 890120. 400. MB

DIABATIC INITIALIZATION

Fig. 2.c

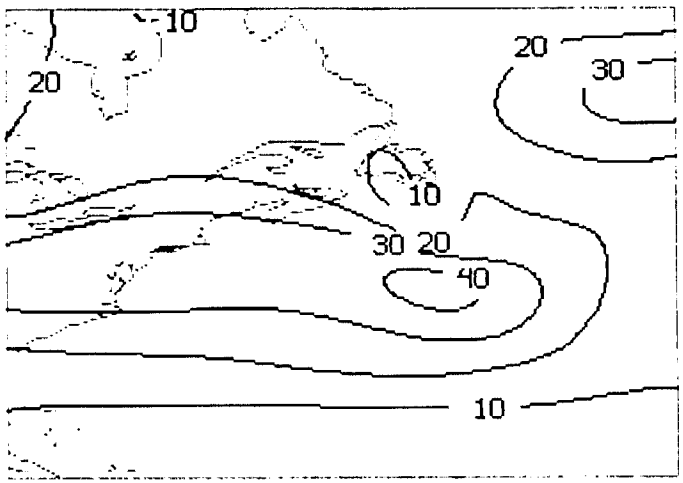

SPD (MPS) TIME 12. DAY 890120. 500. MB 24H FORECAST

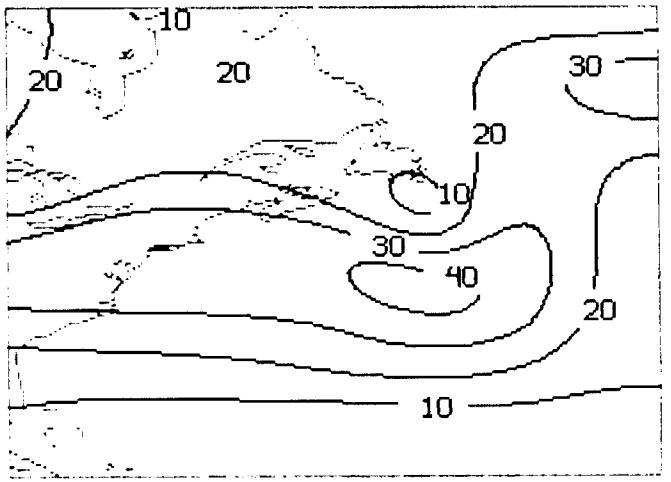

SPD (MPS) TIME 12. DAY 890120. 500. MB 12H FORECAST COLD

WINDSPEED

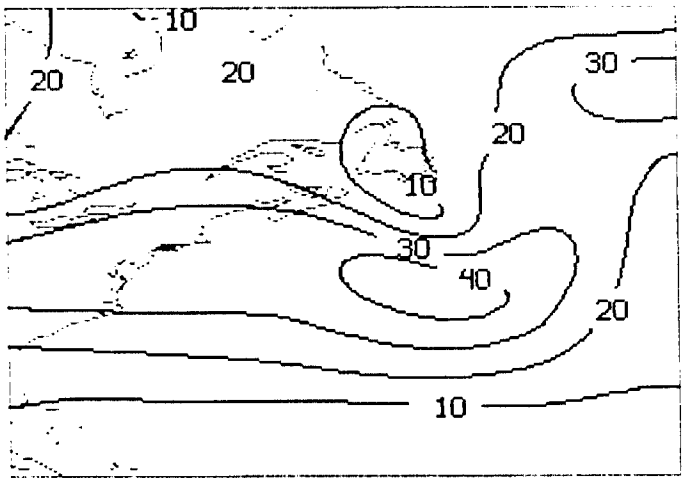

SPD (MPS) TIME 12. DAY 890120. 500. MB EXTERNALLY FORCED 2H

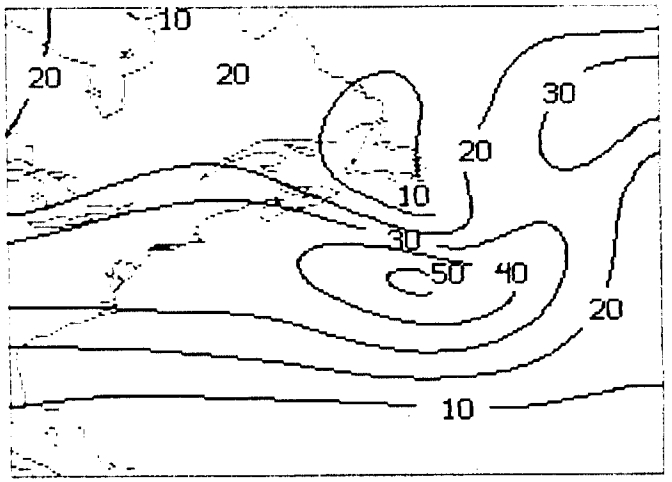

SPD (MPS) TIME 12. DAY 890120. 500. MB EXTERNALLY FORCED 4H

Fig 21

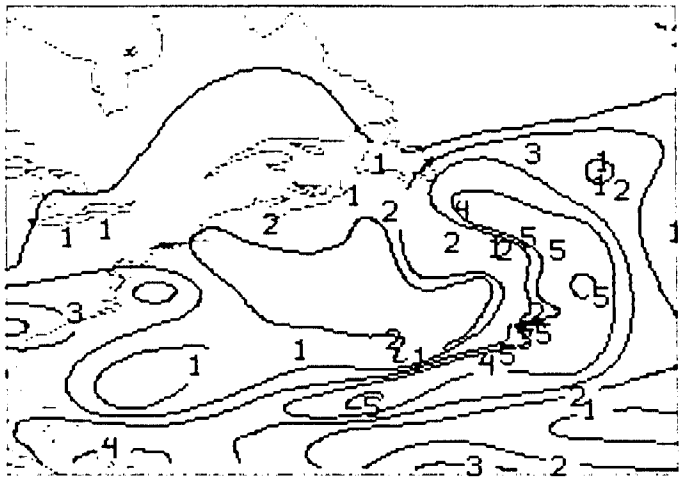

MIXR (GPKG) TIME 12. DAY 890120. 700. MB 24H FORECAST

MIXR (GPKG) TIME 12. DAY 890120. 700. MB 12H FORECAST COLD

MIXING RATIO

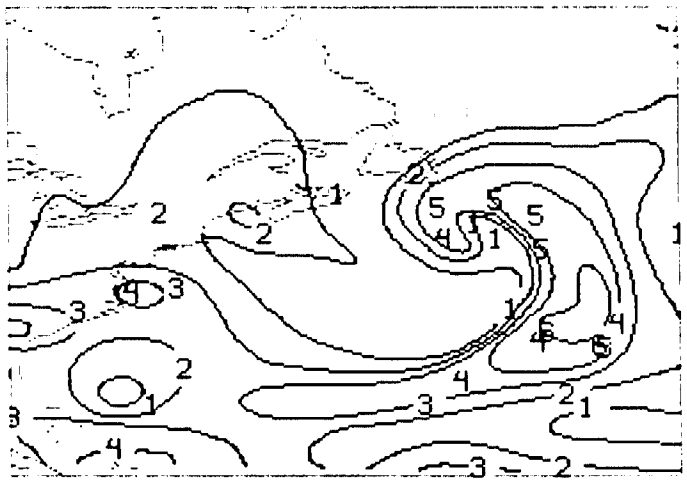

MIXR (GPKG) TIME 12. DAY 890120. 700. MB EXTERNALLY FORCED 2H

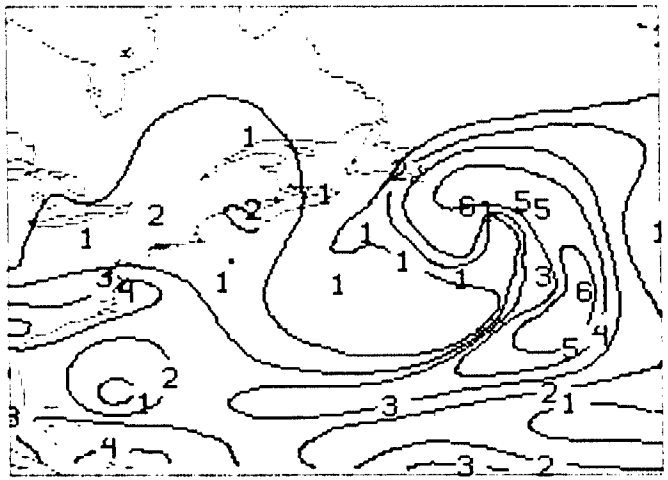

MIXR (GPKG) TIME 12. DAY 890120. 700.MB EXTERNALLY FORCED 4H

Fig 22

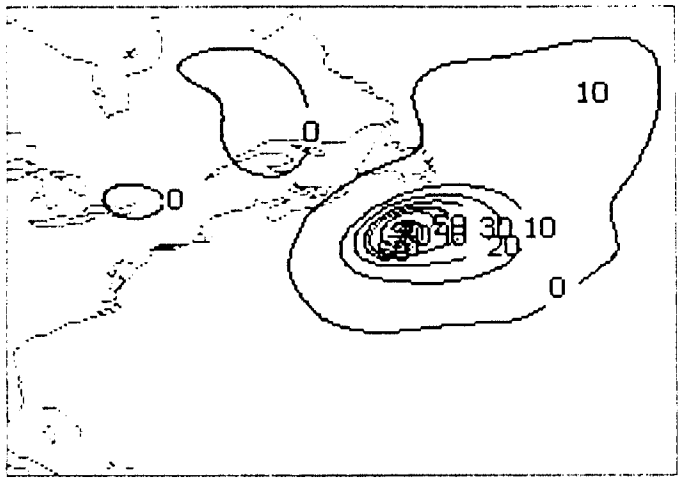

PPTN (MM) TIME 12. DAY 890120. 24H FORECAST

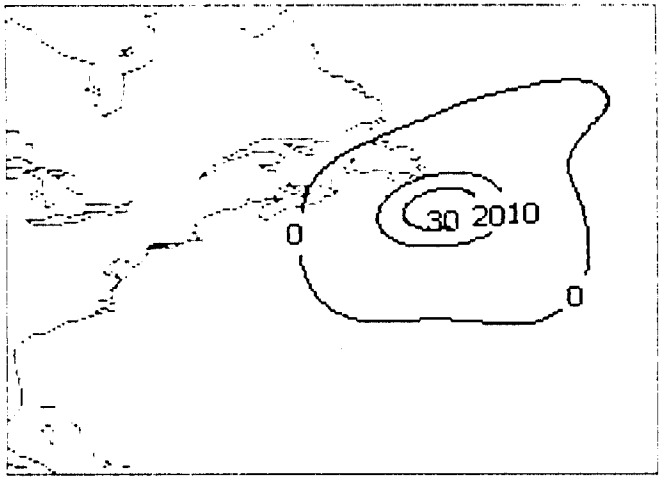

PPTN (MM) TIME 12. DAY 890120. 12H FORECAST COLD START

RAINFALL

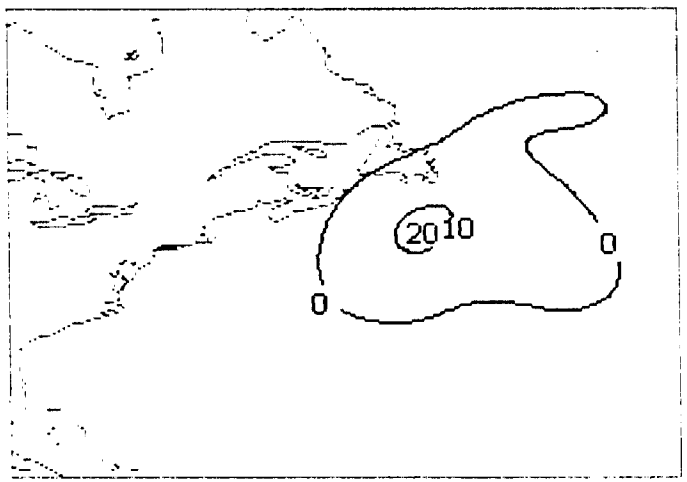

PPTN (MM) TIME 12. DAY 890120. EXTERNALLY FORCED 2H

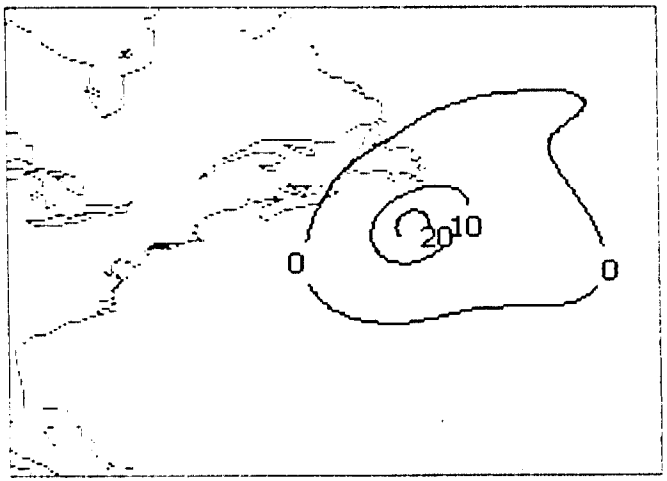

PPTN (MM) TIME 12. DAY 890120. EXTERNALLY FORCED 4H

Fig 23

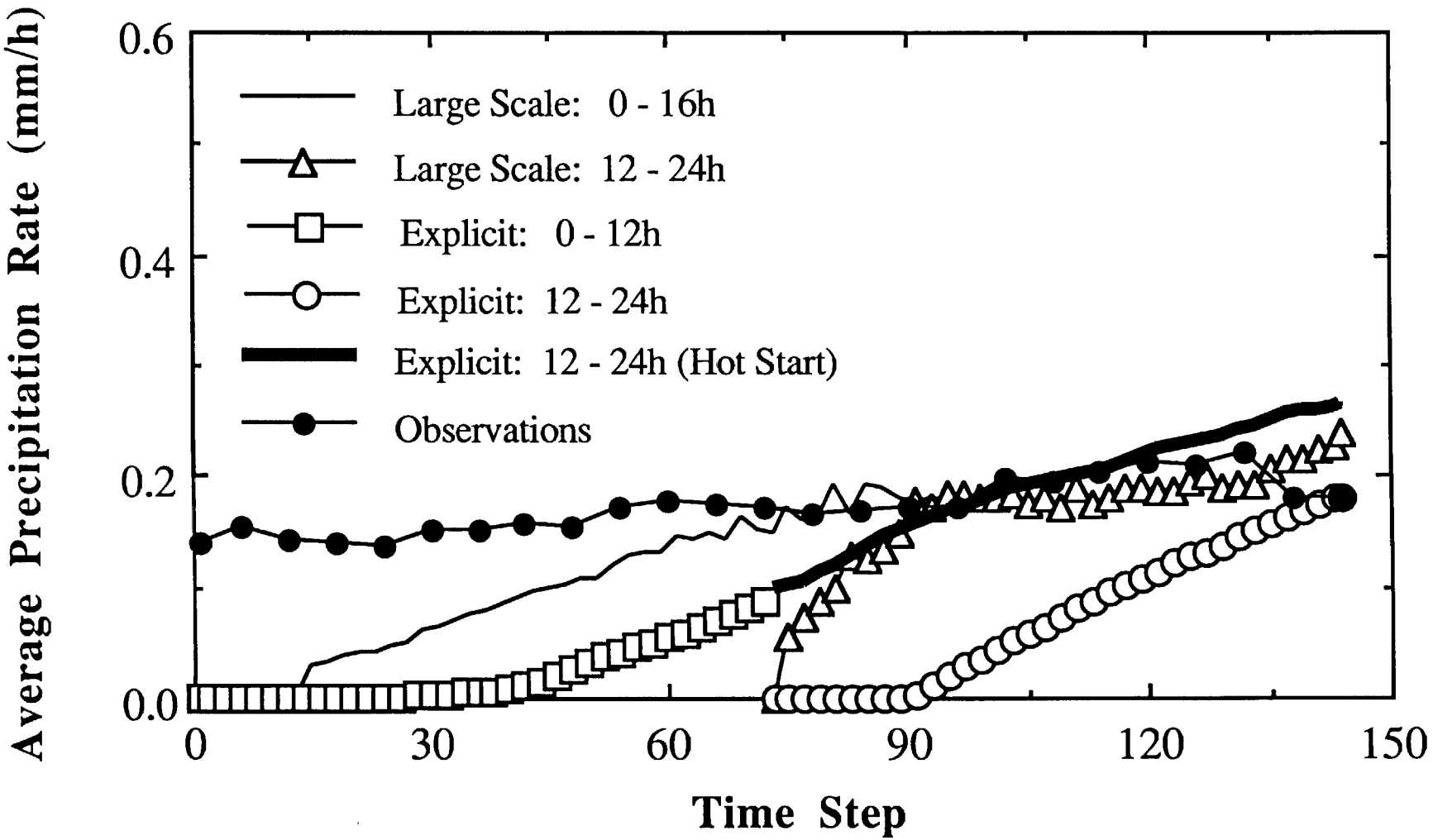
Average Precipitation Rate (mm/h)
0.6
0.4
0.2
0.0
0
30
60
90
120
150
Time Step
Large Scale: 0 - 16h
Large Scale: 12 - 24h
Explicit: 0 - 12h
Explicit: 12 - 24h
Explicit: 12 - 24h (Hot Start)
Observations

Fig 24

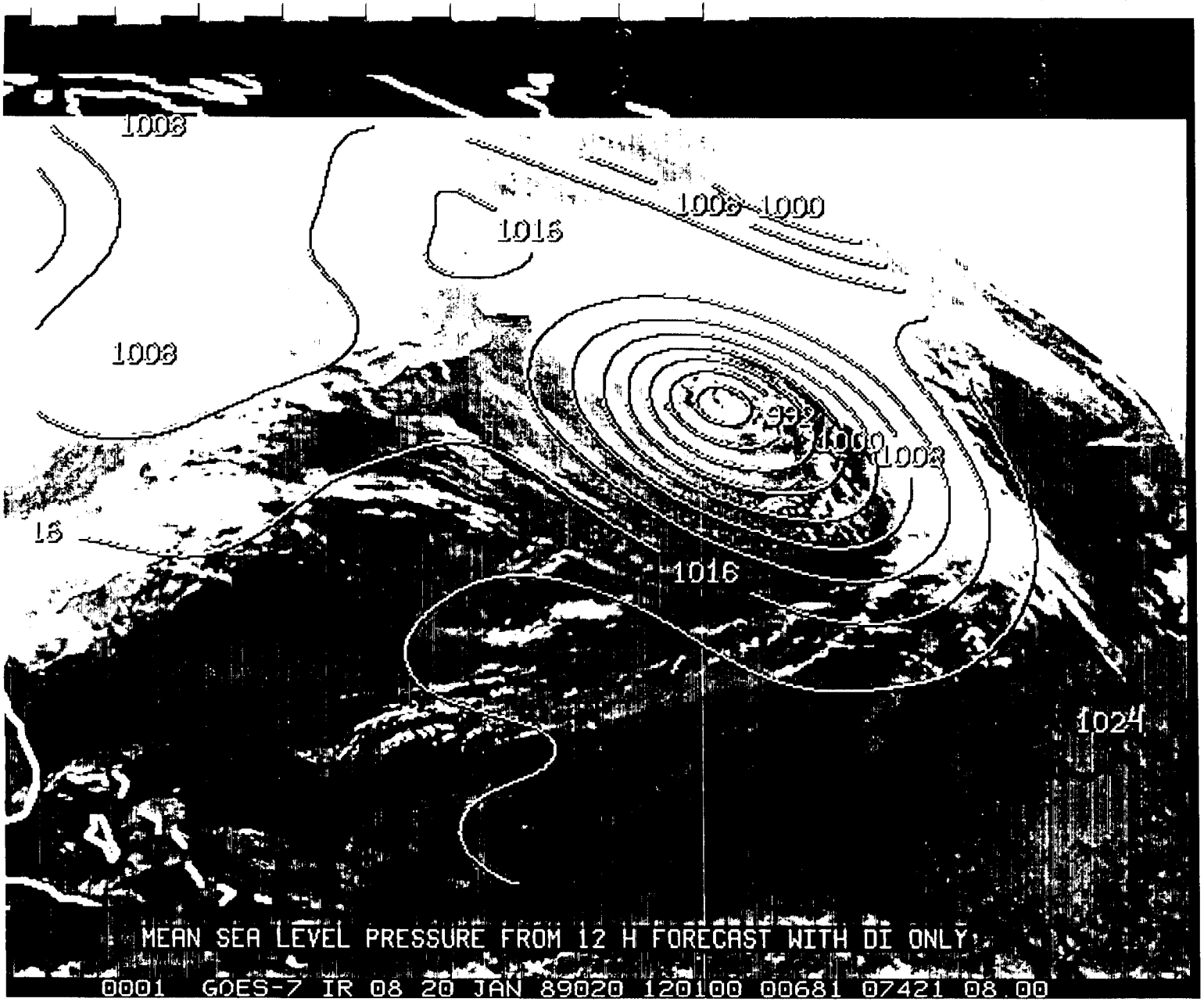
1008
1008 1000
1016
1008
992
1000
1008
16
1016
1024
MEAN SEA LEVEL PRESSURE FROM 12 H FORECAST WITH DI ONLY
0001 GOES-7 IR 08 20 JAN 89020 120100 00681 07421 08 00

Fig 25

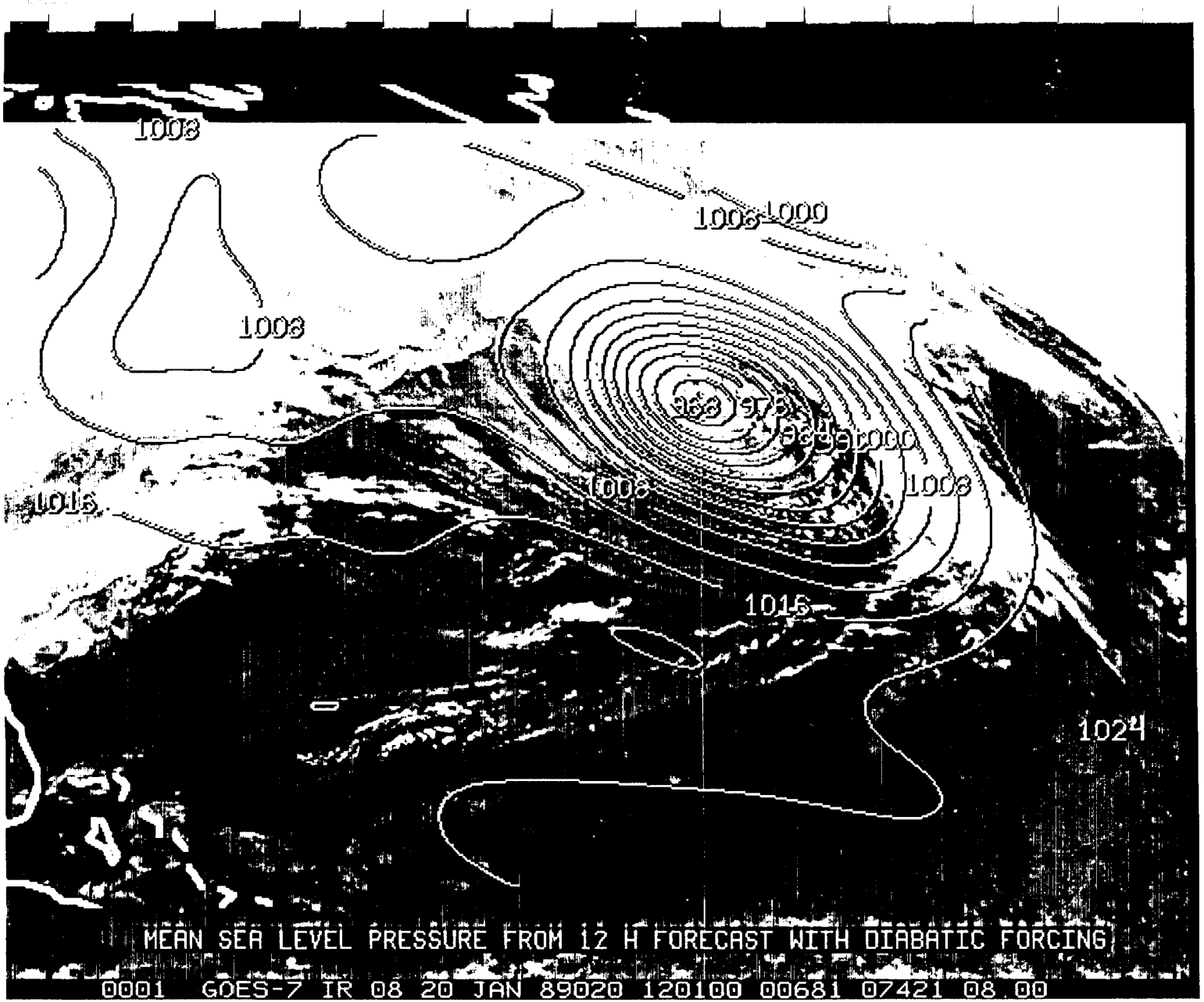
1008
1008
1000
1008
1008
1008
1016
1016
1024
MEAN SEA LEVEL PRESSURE FROM 12 H FORECAST WITH DIABATIC FORCING
0001 GOES-7 IR 08 20 JAN 89020 120100 00681 07421 08 00

Fig 3c

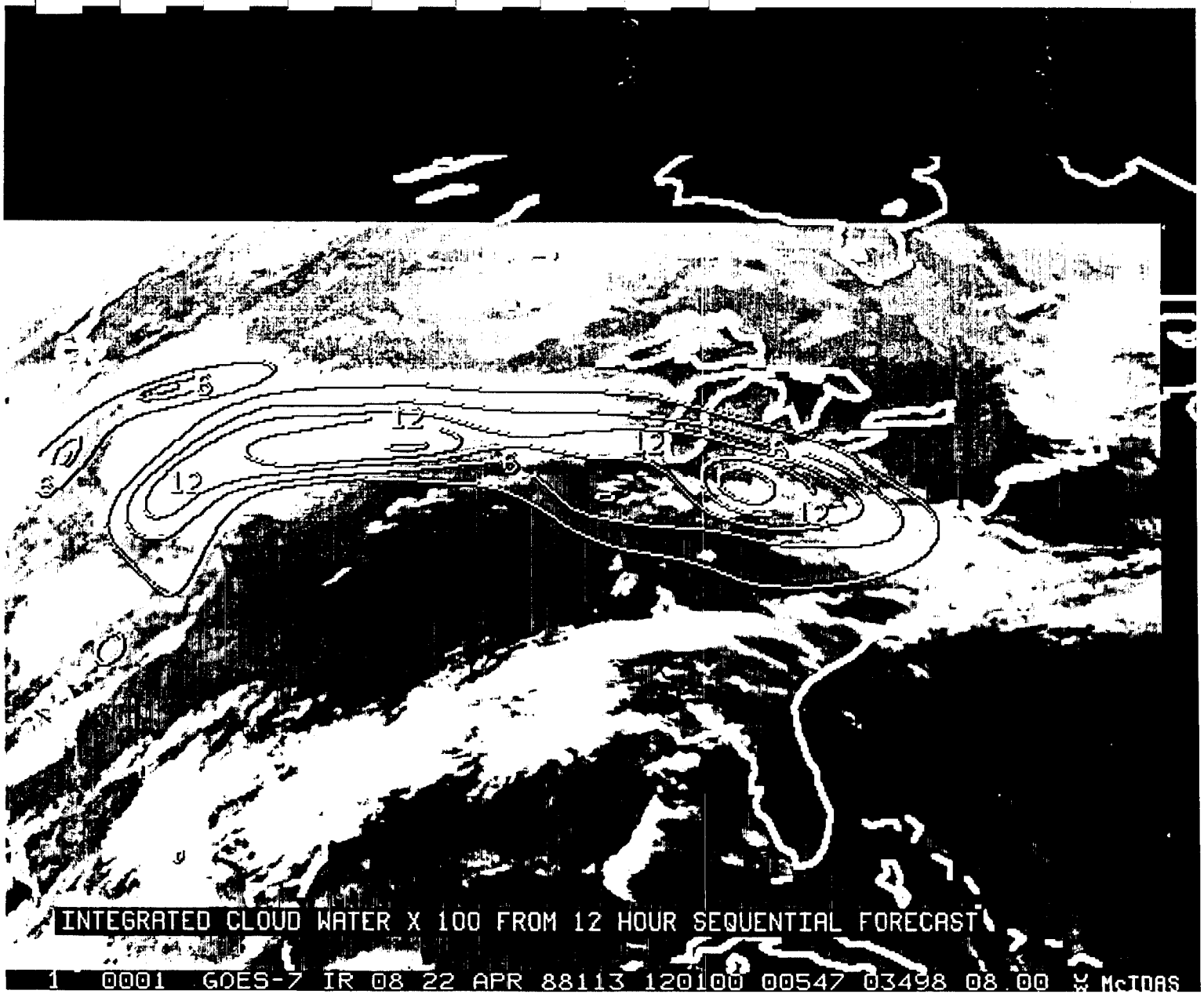
6
12
12
6
12
6
12
INTEGRATED CLOUD WATER X 100 FROM 12 HOUR SEQUENTIAL FORECAST
1 0001 GOES-7 IR 08 22 APR 88113 120100 00547 03498 08 00 McIDAS

Fig 27

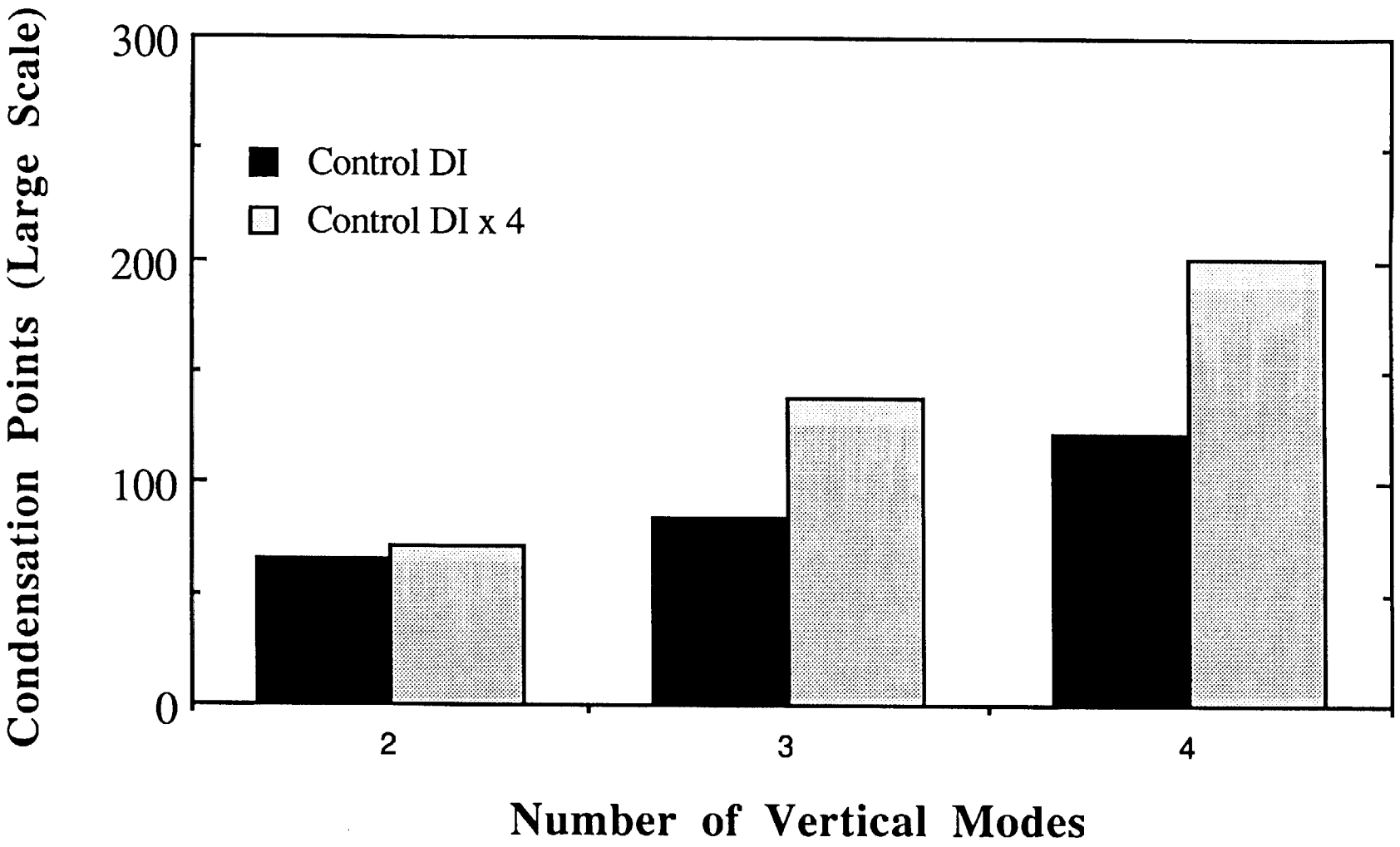
Condensation Points (Large Scale)
300
200
100
0
Control DI
Control DI x 4
2
3
4
Number of Vertical Modes

Fig 28

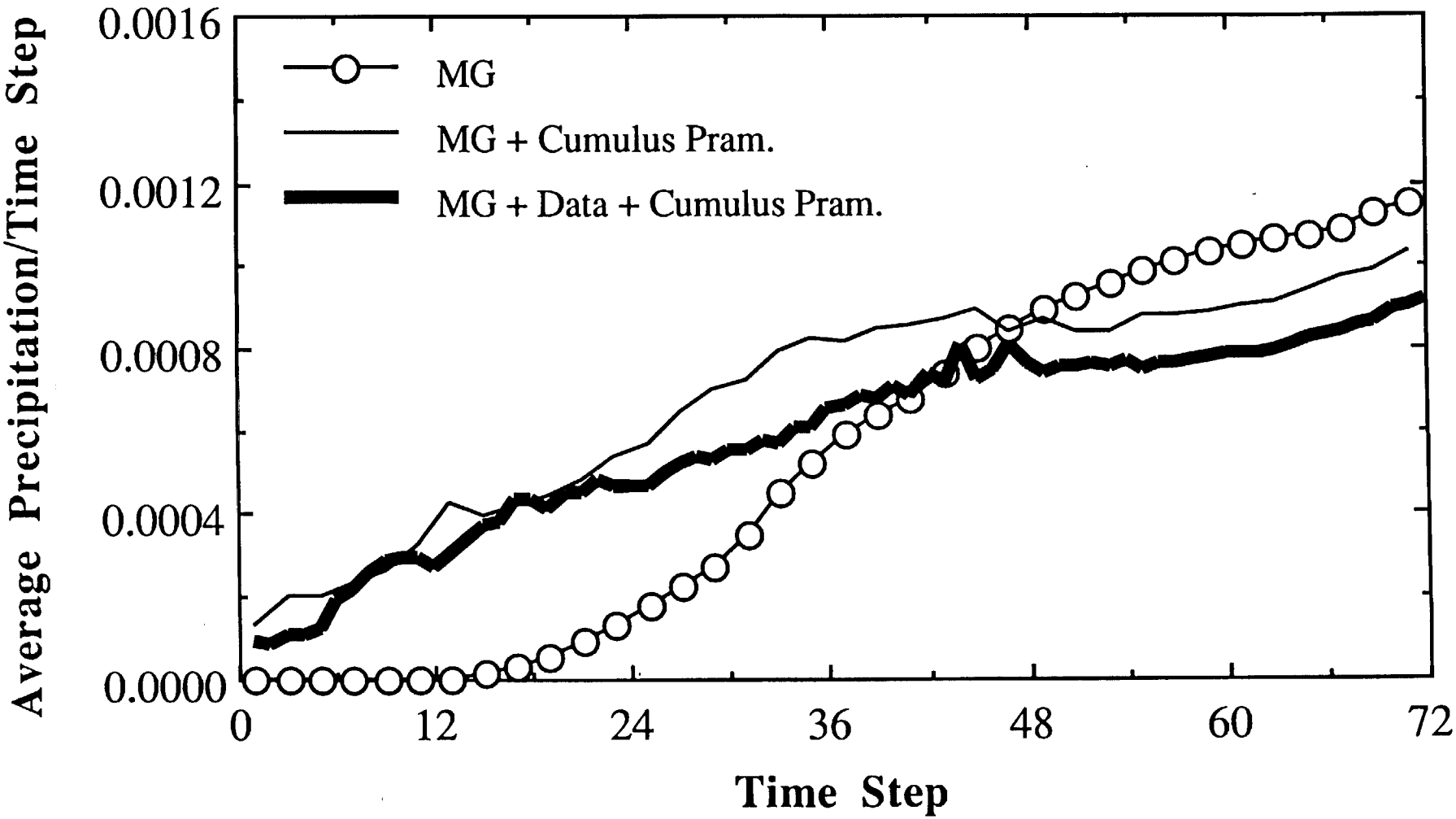
MG
MG + Cumulus Pram.
MG + Data + Cumulus Pram.
Average Precipitation/Time Step
0.0016
0.0012
0.0008
0.0004
0.0000
0
12
24
36
48
60
72
Time Step

Fig 29

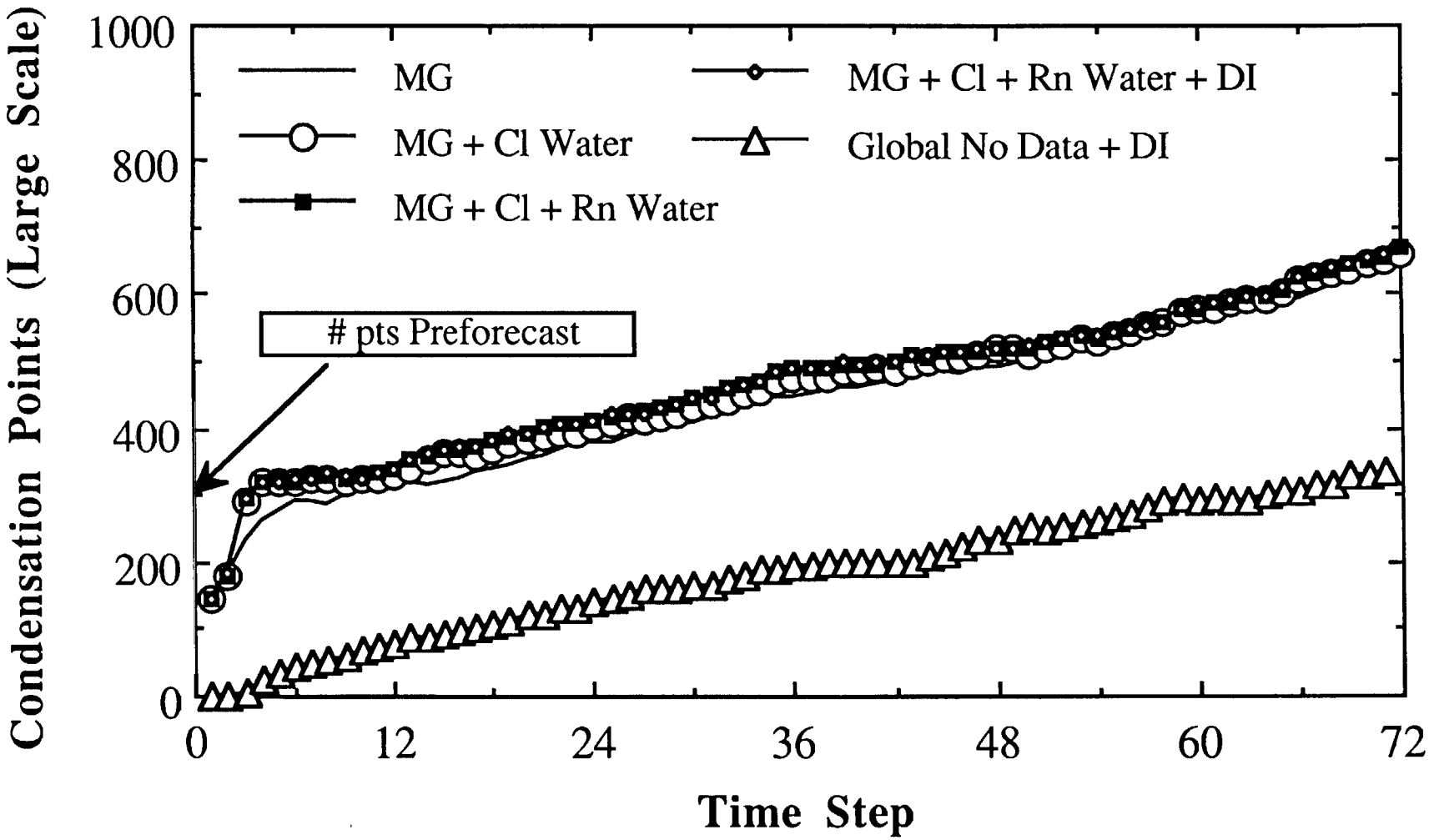
Condensation Points (Large Scale)
1000
800
600
400
200
0
0
12
24
36
48
60
72
Time Step
MG
MG + Cl Water
MG + Cl + Rn Water
MG + Cl + Rn Water + DI
Global No Data + DI
pts Preforecast

Fig. 3a

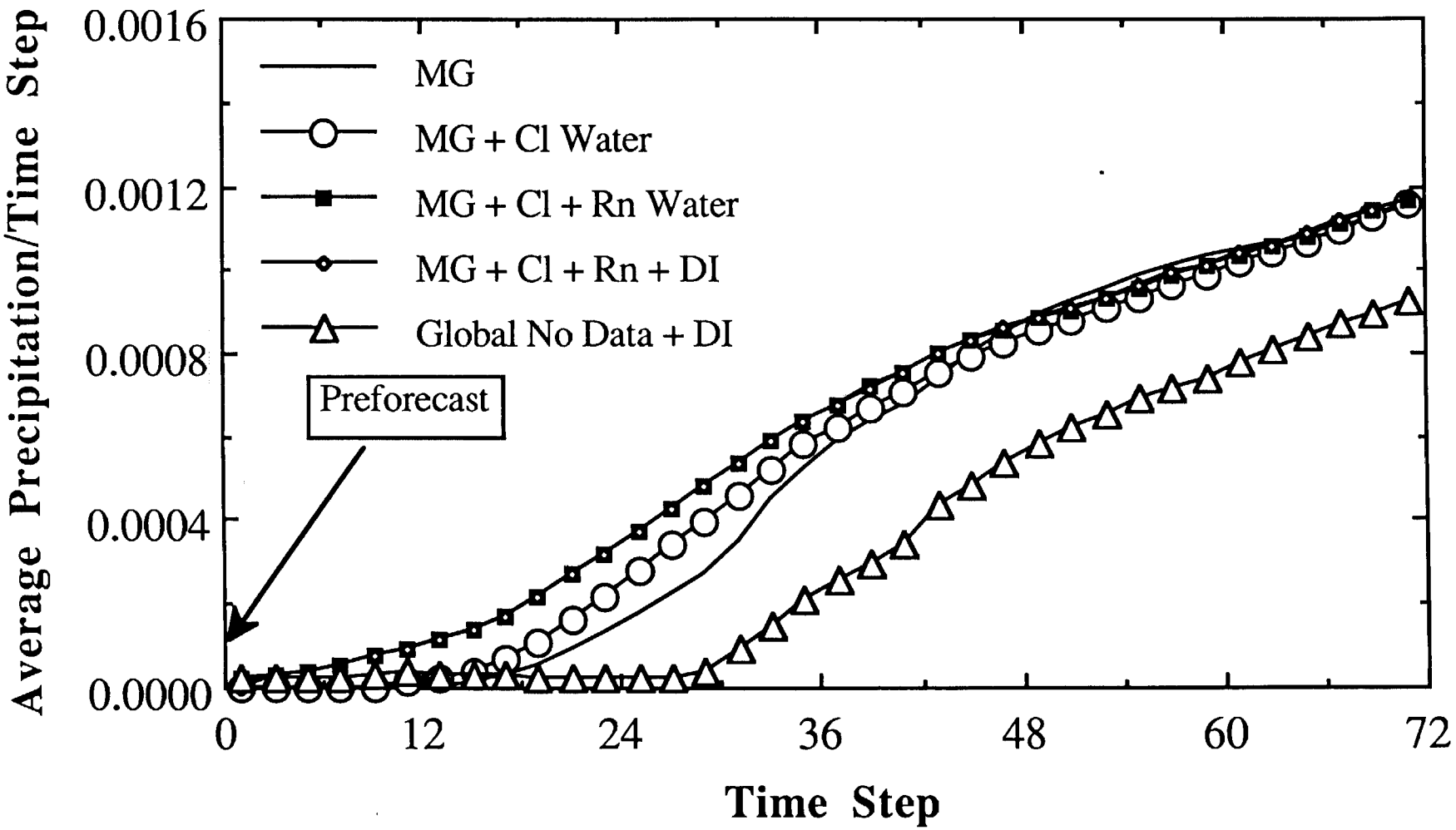
Average Precipitation/Time Step
0.0016
0.0012
0.0008
0.0004
0.0000
MG
MG + Cl Water
MG + Cl + Rn Water
MG + Cl + Rn + DI
Global No Data + DI
Preforecast
0
12
24
36
48
60
72
Time Step

Fig 31

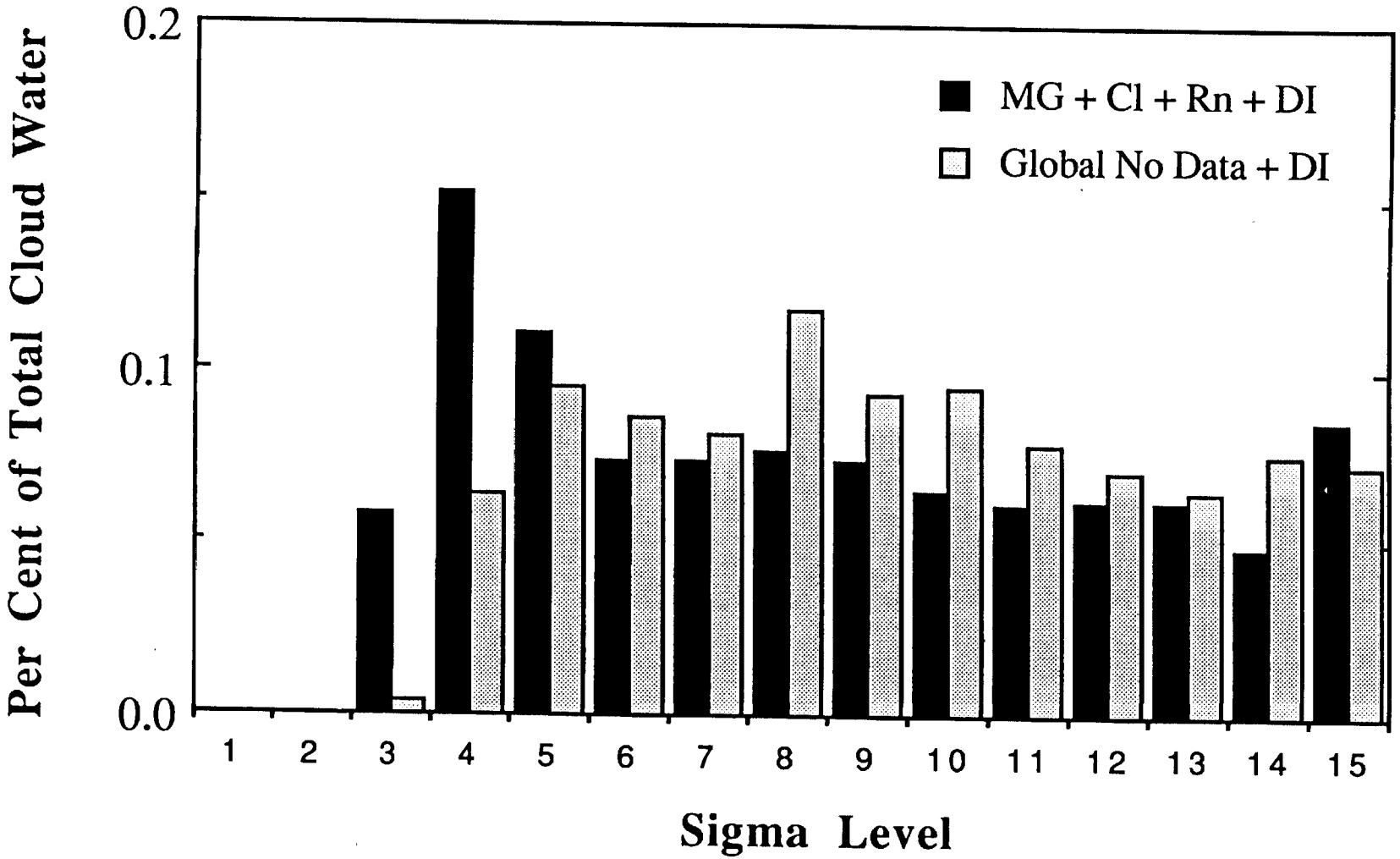
0.2
0.1
0.0
Per Cent of Total Cloud Water
MG + Cl + Rn + DI
Global No Data + DI
1
2
3
4
5
6
7
8
9
10
11
12
13
14
15
Sigma Level

Fig 32

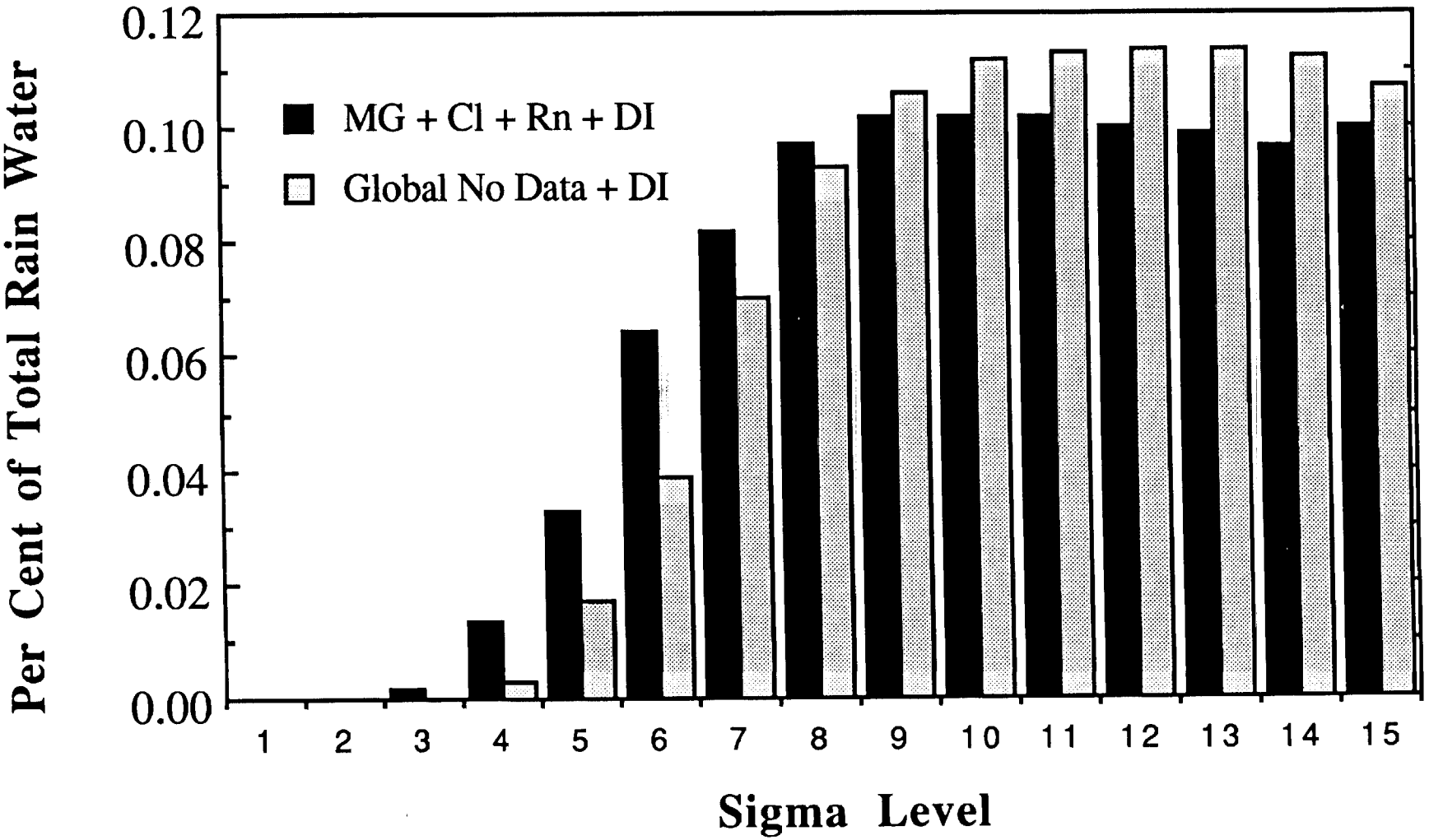
Per Cent of Total Rain Water
0.12
0.10
0.08
0.06
0.04
0.02
0.00
MG + Cl + Rn + DI
Global No Data + DI
1
2
3
4
5
6
7
8
9
10
11
12
13
14
15
Sigma Level

Fig 33